Microfluidic Loading Strategy for 7,8-Dihydroxyflavone and Functional Evaluation

By

ABIGAIL HUMPHRIES
THESIS

Submitted in partial satisfaction of the requirements for the degree of

MASTER OF SCIENCE

in

Biomedical Engineering

in the

OFFICE OF GRADUATE STUDIES

of the

UNIVERSITY OF CALIFORNIA

DAVIS

Approved:

Randy Carney, Co-Chair

Aijun Wang, Co-Chair

Steven George

Committee in Charge

2026

Acknowledgements

This thesis would not have been possible without an array of people who have supported me both academically and personally throughout my time at the University of California, Davis contributing to both my professional and personal development.

I would like to thank my committee members for their mentorship and guidance in this pursuit. I would like to thank Professor Randy Carney for his guidance throughout my degree and expertise in all things related to liposome and extracellular vesicle. I would like to show my gratitude to Professor Aijun Wang for providing the basis for the work on this project and neuroprotection. To Professor Steve George, I am thankful for his teaching and mentorship throughout my education and extracurriculars at UC Davis.

A handful of amazing people have also made my time at UC Davis an exceptional experience and carried me through the tribulations of graduate school. Gratitude is extended to my fellow graduate students Napsia, Eden, Jared and Nik for our many game nights and study sessions together. To my family and James, I am thankful for your unwavering support throughout my education.

List of Figures

Abstract

7,8-Dihydroxyflavone (7,8-DHF) is a tyrosine receptor kinase B agonist that has been demonstrated to show therapeutic promise for treatment of several neuropsychiatric disorders, as well as injuries, of the central nervous system. Unfortunately, there is a gap in the delivery system for this drug as its pharmacokinetics could be improved upon by increasing its clearance time, while retaining the ability to affect neuronal cell types towards protection and proliferation. To this end, the loading of liposomes and extracellular vesicles with the small molecule has been posited as an effective delivery mechanism. As a hydrophobic drug, a scalable, efficient 7,8-DHF loading strategy that simultaneously produces homogenous particles for accurate therapeutic dosing is currently an unmet need. In service of this problem statement, we propose the optimization of the microfluidic-based NanoAssemblr Ignite LNP formulation platform first for the loading of a DOPC and cholesterol-based liposome, then incorporating within a hydrophobic drug and fluorophore labelled lipid. Results show the ability to effectively tune parameters to generate liposomes that encapsulates and retains the function of 7,8-DHF with a size of approximately 120 nm measured on NTA and a polydispersity index of 0.221 when measured through DLS. These liposomes also function better in a SY5Y neuroprotection assay than the free drug comparison when measuring cell count, area and an over 6-fold increase in neuron length between drug-loaded liposome and PBS control.

Chapter 1: Introduction

1.1 Trkb Agonists

Tyrosine receptor kinase B (TrkB) is a transmembrane protein expressed in neuronal cells that acts as a receptor for neurotrophic compounds like the protein brain-derived neurotropic factor (BDNF) and small molecule 7,8-Dihydroxyflavone (7,8-DHF). When activated, the signaling pathways from TrkB play a role in neuronal survival and function, with demonstrated neuroprotective effects through induction of the PLCγ, PI3K and MAPK/ERK pathways illustrated in Figure 1.1 [1, 2]. From these pathways, increased BDNF leads to more dendrite and axonal growth, as well as increased neuronal proliferation, differentiation and survival. For this reason, drug delivery of both BDNF and 7,8-DHF are under consideration for therapeutics utilized in the treatment of several neuropsychiatric diseases and injuries of the central nervous system such as Alzheimer's, Parkinson's, depression and memory impairment, as well as traumatic brain injury, neural tube defects and intellectual disabilities [3].

1.2 7,8-Dihydroxyflavone

The small molecule 7,8-DHF is a type of flavonoid, which is a class of plant metabolites that have been broadly determined to possess several pharmacological benefits. To the effect of neuroprotection, 7,8-DHF is also able to cross the blood brain barrier (BBB) but, unfortunately, has a pharmacokinetically unfavorable profile, with a half-life of 134 minutes in mouse models, a low bioavailability of roughly 5% when administered through oral gavage, and additionally binds to human serum albumin and other circulating proteins, decreasing the amount of free drug able to exhibit a therapeutic effect and decreases the time it takes to clear through circulation [4,5]. 7,8-DHF is cleared biologically through glucuronidation, sulfation, and methylation,

making it more hydrophilic and easily excreted by the kidneys, and much faster than CYP enzymatic degradation. This low bioavailability and protein interaction is largely due to the molecule's hydrophobicity, meaning it is difficult to dissolve in aqueous solution, as well has strong interactions with hydrophobic domains in proteins [6,7].

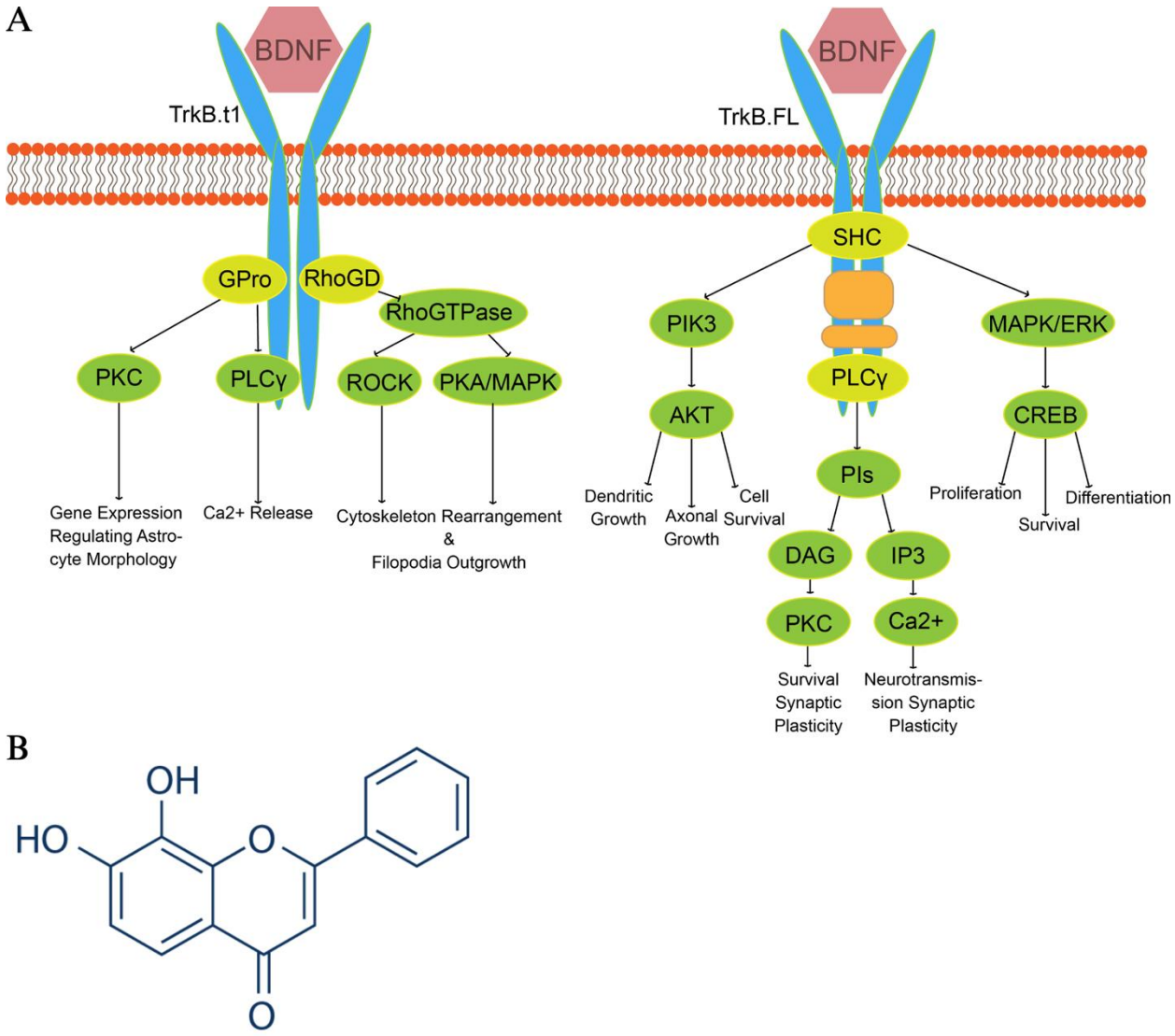

Figure 1 – TrkB and agonist 7,8-DHF. (A) Signaling pathway for TrkB and their downstream effects on the CNS. (B) Chemical structure of 7,8-DHF [6,7]. Created with BioRender.com.

To compensate for these detriments, a drug delivery platform must be developed that is able to increase circulation time and drug bioavailability, while still retaining the ability to cross the blood-brain barrier. One avenue of research that has been pursued in drug delivery to address these deficiencies is encapsulation in either liposomes or extracellular vesicles (EVs). Liposomes are artificially produced lipid membrane bound vesicles which can be formed, and drug loaded through numerous strategies [8]. Conversely, EVs are naturally derived and isolated from cells, with variable characteristics in size, cargo, function and biogenesis, even within a sample derived from a single cell population.

1.3 Liposomes

Liposomes are bilayer vesicles that are generated through hydrophobic interactions of lipids that can encapsulate hydrophilic solutions due to the hydrophilic head group and hydrophobic tails. These vesicles can have a variety of properties, tunable by the characteristics of the lipid constituents, as well as their size, surface charge, lamellarity and method of formation. From these characteristics, several classifications can be endowed to a population of liposomes based on size, surface charge and lamellarity [8].

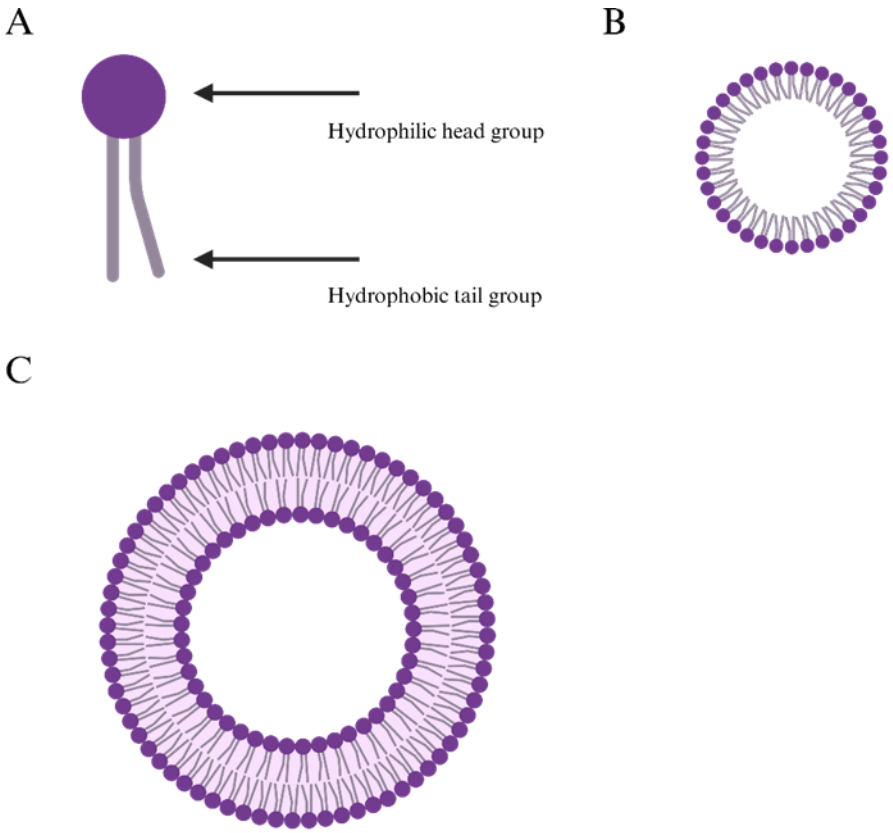

Figure 2 – General lipid and liposome structure. (A) Lipids are split into two regions: the hydrophilic head group and the hydrophobic tail groups. (B) Lipids that assemble into hollow spherical monolayers are micelles. (C) Lipids that assemble into hollow spherical bilayers are liposomes. Created with BioRender.com.

1.3.1 Liposome Characterization: Size and Polydispersity Index

Liposomes can be classified broadly by size into small unilamellar vesicles (SUVs), large unilamellar vesicles (LUVs) and giant unilamellar vesicles (GUVs). The difference is SUVs are in the range of the lowest a bilipid membrane can be, around 20 nm, up to 100 nm, and LUVs are most commonly in the 100-200 nm range but can range to 1000 nm. Anything beyond that 1000 nm mark is referred to as a giant unilamellar vesicle. Size has influence on several properties including uptake and stability. Smaller vesicles are not practical for long-term applications as they will commonly fuse into larger vesicles. While this problem is not associated with larger vesicles, the lower membrane curvature of larger liposomes is associated with less membrane fusion and decreased cellular uptake of liposomes [9].

1.3.2 Liposome Characterization: Surface Charge

Liposome surface charge is measured through zeta potential, which gives either a positive, negative or neutral value. Zeta potential in liposomes is modulated through lipid composition, where lipids with charged head groups, both anionic and cationic, contribute to the overall positive or negative value [10]. Surface charge is significant for liposomes because it directly corresponds to uptake mechanisms, which vary between cell types [11].

1.3.3 Liposome Characterization: Lamellarity

There are three classifications of lamellarity that vesicles can be divided into: unilamellar, multilamellar, and multivesicular. As shown in Figure 3, unilamellar vesicles are bodies made from one bilayer, with a hollow, aqueous core, while multilamellar vesicles are concentric bodies of multiple bilayers and multivesicular are nonconcentric membranes encapsulated by a larger liposome [9].

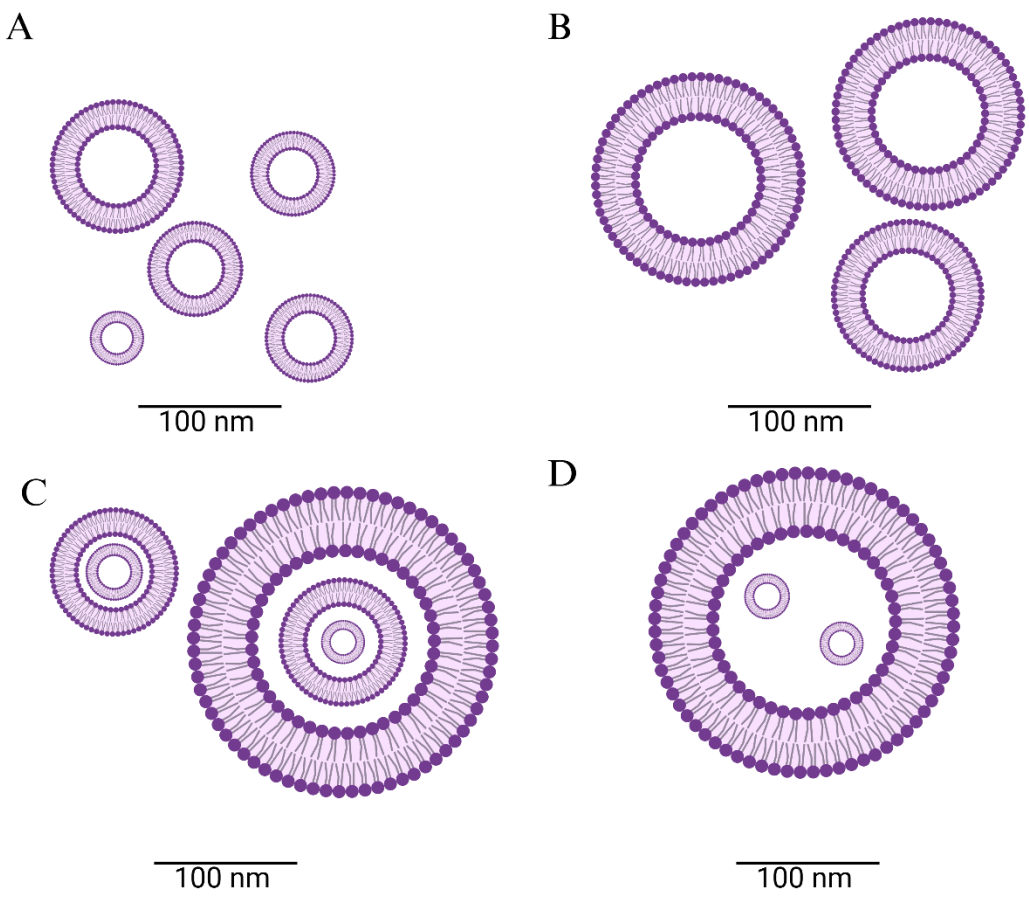

Figure 3 – Liposome sizing and lamellarity. (A) Small unilamellar vesicles (SUVs) are structures composed of one bilayer membrane under the size of 100 nm. (B) Large unilamellar vesicles (LUVs) are like SUVs but are larger than 100 nm and under 1000 nm. (C) Multilamellar vesicles are made from more than one concentric lipid bilayer. (D) Multivesicular bodies are like multilamellar liposomes without concentricity of their bilayers. Created with BioRender.com.

1.4 Liposome Formation and Loading

To prepare and drug load liposomes, there are several methods that have been previously employed to varying degrees of success that are broadly lumped into active and passive synthesis mechanisms [12].

1.4.1 Thin Film Hydration

Many techniques for liposome generation and loading build off thin film hydration. Under argon or nitrogen gas, lipids suspended in an organic solvent (i.e. chloroform, ethanol, methanol) have their solvent evaporated off to create a thin membrane on a glass flask. After complete removal

of the organic solvent, the film is rehydrated with an aqueous solution above the lipid's transition temperature. Though liposomes will form in these conditions, their characteristics will be largely heterogenous with unspecific size and a large PDI [9, 13].

1.4.2 Sonication

The easiest sizing procedure that can be done after thin film hydration is sonication. Introduction of sonic energy into the solution via, most commonly, a bath sonicator, will commonly give particles on the lower possible size, in the range of 15-50 nm SUVs, but is commonly also contaminated with larger vesicles. There are several downsides to this method of formation including requiring subsequent centrifugation to remove large vesicles, liposome instability, large batch variability, and poor encapsulation of hydrophobic compounds. Since these liposomes are largely unstable due to their size and high degree of curvature, they will commonly spontaneously fuse to create larger vesicles in storage below their phase transition temperature. This can also lead to the need to centrifuge after formation to remove this subset of liposomes. In addition, there is a multitude of parameters that contribute to liposome characteristics in this procedure, such as sonication time, power, temperature, and lipid concentration which leads to variability between batches. It is also worth noting that since this procedure is done without an organic solvent, there is poor solubility and encapsulation efficiency of hydrophobic compounds [9, 12, 13].

1.4.3 Extrusion

Another post-processing sizing method is membrane extrusion, where the aqueous lipid solution is passed through a polycarbonate nanoporous membrane. Passes through the membrane restrict the size of the liposomes, and the addition of a heating block allows for resizing above phase transition temperatures. Though this gives a much more monodisperse population and more

tunable sizing, downsides to this include mechanical technical difficulties, reduced scalability, high time demand and poor solubility of hydrophobic compounds. This syringe system has several points of failure and technical limitations like clogging and leaking systems which can lead to technical difficulties and inconsistencies. Since these systems are passing aqueous mixtures between syringes less than 1 mL, the system cannot handle high lipid concentrations or volumes leading to reduced scalability. Aside from the time required to set up the syringe system, manual extrusion itself can require time and physical exertion with smaller pored membranes, usually requiring 11-21 passes through the membrane to homogenize the liposomes. Much like sonication, there is poor solubility and incorporation of hydrophobic compounds since lipids are being suspended in an aqueous phase [9, 12, 13].

1.4.4 Detergent Removal

The detergent removal method for liposome formation is the successive removal of a detergent from a lipid mixture leading to micelle formation that progresses to vesicles with continual lowering of the solvent concentration. This can happen through dilution or dialysis, with the benefits of these methods being tunability in particle size and shape, which is affected by the rate at which the detergent is removed and the initial ratio between phospholipid and detergent. With the nature of this formation method, the downsides accompanying are low encapsulation efficiency of both hydrophobic and hydrophilic compounds, low liposome concentrations and necessary postprocessing detergent removal steps. In diluting the solvent, both the lipid and any drug being encapsulated is also diluted, which can lead to poor liposome concentration and encapsulation efficiency. In dialysis methods, drug encapsulation may also be hindered as passive diffusion over time leads to leakage from the liposomes. For biological applications, the

presence of these strong detergents can be detrimental and postprocessing steps may be needed to remove trace amounts of these compounds to make them safe for therapeutics [9, 12, 13].

1.4.5 Solvent Injection

Like detergent removal, the solvent injection method of liposome formation starts with the dissolution of lipids within an organic solvent but differs as the lipid solution is then introduced rapidly to an aqueous solution resulting in the organic solvent's dilution below the critical concentration where lipids are dissociated. In this formation method, lipids self-assemble into raft-like fragments upon introduction to the aqueous phase which are then further influenced to fuse into liposomes by solvent removal through dialysis or evaporation. Positive attributes conferred by this method are high encapsulation efficiencies of hydrophobic drugs with the ability to create SUVs with a low PDI. In addition, hurdles to its scalability have been alleviated with the use of pipetting robots to shorten production time and decrease costs allowing for higher throughput screening of liposomal formulations. Downsides include low encapsulation of hydrophilic drugs, and many parameters that influence liposomal properties including aqueous pH and viscosity, temperature, stirring speed, ethanol concentration, and osmolality [9, 12, 13].

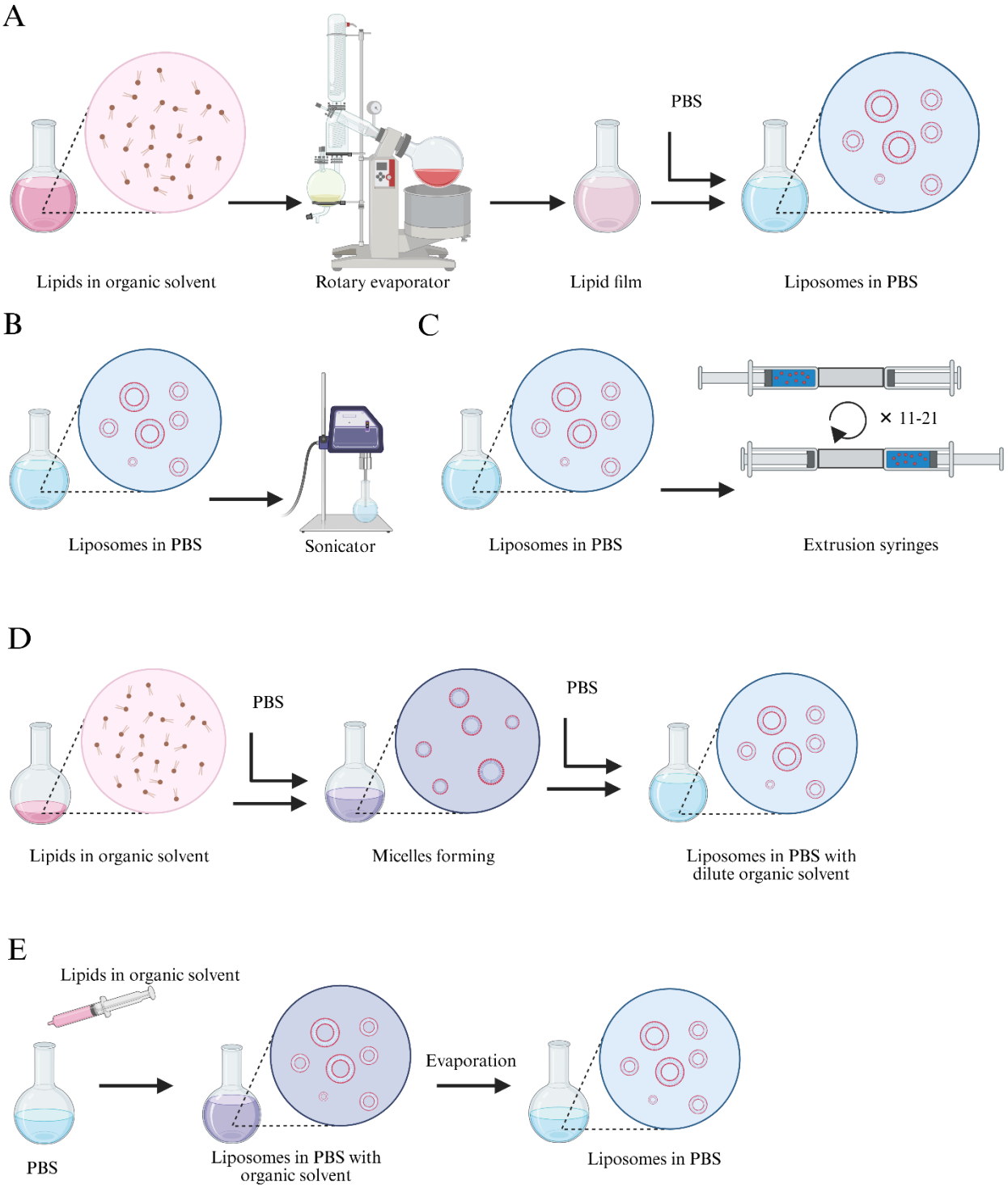

Figure 4 – Traditional liposome formation methods. (A) Liposome formation method of thin film hydration starts with lipids in an organic solvent, evaporated through rotary evaporation or under nitrogen gas to form a lipid film. The film is rehydrated in PBS or another aqueous solvent. (C) Extrusion through a membrane after thin film hydration results in more uniformly sized liposomes. (D) Detergent removal progressively dilutes lipids in their organic solvent leading to self-assembly into micelles then liposomes as the concentration lowers. (E) In solvent injection, lipids in their organic solvent are supplied to an aqueous solvent rapidly lowering their concentration followed by evaporation to remove organic solvent and purify liposomes. Created with BioRender.com.

1.5 Microfluidic Formation and Loading

As translational requirements for liposomes in healthcare require a homogenous, and low PDI population of nanoparticles with the ability to load a diverse library of drugs and cargos, the negative aspects of previously employed liposome formulation methodologies may be overcome by microfluidics. The basis of all microfluidic platforms is the combination of an aqueous phase and a lipid containing organic phase, where the thin film hydration method is modified to result in resuspension in an organic solvent, like ethanol or dimethyl sulfoxide (DMSO). Along with some more rudimentary versions, like a T-junction, mixers exist that employ complex microscopic geometry, such as the herringbone or toroidal pattern shown in Figure 5, to increase turbulent flow at low volumes [14].

1.5.1 Microfluidic Dynamics and Governing Equations

Flow can be characterized by the Reynolds number, where a smaller number is more indicative of laminar flow in particles flow more like parallel layers with little mixing between layers. In turbulent flow, particles are constantly changing speed and direction through interactions with other particles and are indicated by a higher Reynolds number. The Reynolds number is governed by the fluid density, flow speed, the length of the characteristic being evaluated and fluid viscosity. In microfluidic devices, the Reynolds number can be particularly small since we are working with high flow rates to decrease particle size, and the ethanol phase is even less viscous than water. To overcome this, newer iterations have included additional geometries to induce turbulence, such as the staggered herringbone and bifurcating mixers. In the staggered herringbone mixer, asymmetric grooves induce stretch and fold the fluid, rotating the fluid back on itself and decreasing the distance between fluid layers. The bifurcating mixer functions by exerting centrifugal force on the fluids to create counter rotating vortices, increasing a type of

secondary fluid flow called Dean flow. In this mixing, turbulent flow is induced through an increased fluid inertia or by decreasing the radius of the channel around the circular motifs. For Dean numbers lower than approximately 40 to 60, calculated by the equation in Figure 5, where D is the channel diameter and R_c is the radius of the channel's circular motif, flow can be characterized as laminar. With Dean numbers increasing to 64-75, primary vortices start to develop, and further increases are indicative of instabilities that promote mixing [15, 16].

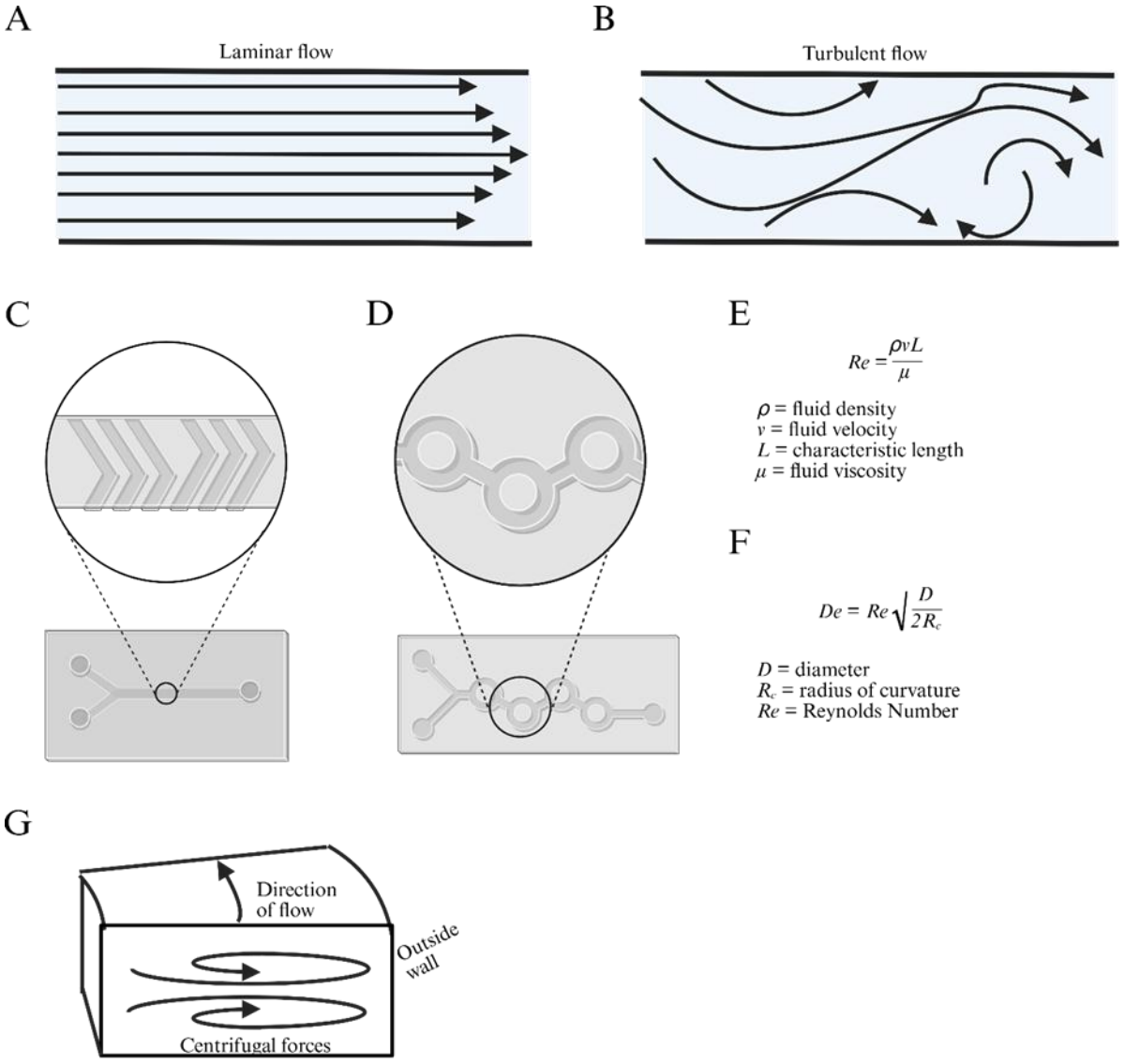

Figure 5 – General fluid dynamics of microfluidics. (A) Laminar flow through a channel. (B) Turbulent flow through a channel. (C) A microfluidic device with a herringbone mixer structure. (D) A microfluidic device with a bifurcating mixer structure. (E) The equation for the Reynolds number, which characterizes laminar versus turbulent flow. (F) The equation for the Dean number, which characterizes flow in curved channels like the bifurcating mixer and is based off the Reynolds number. (G) Dean vortices in a curving channel due to centrifugal forces pushing particles towards the outside wall. Created with BioRender.com.

1.6 Extracellular Vesicles

As mentioned previously, extracellular vesicles are particles naturally excreted by all cell types. Information on their biogenesis, roles in the human body and composition has greatly expanded in hopes of elucidating their possible roles as diagnostic and therapeutic agents. The physical characterizations from liposomes are conserved within EVs, with the cell-derived particles

displaying differences in size, surface charge, and lamellarity, while further adding heterogeneity based on cargos, lipid composition, biogenesis and uptake pathways. Diagnostically, characterizing EVs could lead to advancements in the liquid biopsy, increasing the sensitivity and specificity while decreasing the invasiveness of testing for diseases like cancer by utilizing blood, saliva and urine. Therapeutically, characterizing and modifying EVs could lead to their utilization as next generation drug delivery mechanisms. The loading of liposomes can be improved upon by these vesicles by harnessing native and enhanced EV functions to confer properties such as the ability to cross endothelial barriers, cell-specific targeting, natural biocompatibility, and low immunogenicity, especially in allogenic or autologous applications [17].

1.6.1 Extracellular Vesicle Characterization

EVs are broadly excreted by the cell, however further differentiation by biogenesis pathways can further delineate subpopulations within the class of biological particles. The three main distinct subpopulations are apoptotic bodies, microvesicles, and exosomes, distinguished by their size, in addition to their biogenesis.

The larger classes of vesicles, apoptotic bodies and microvesicles, are both formed by outward membrane blebbing and budding with the contents originating from the cytosol. Apoptotic bodies, which are in the 1-5 μm size range, are generated during apoptosis when cells break down into smaller sacs through outward membrane budding and are typically removed by immune clearing cells through phagocytosis. Microvesicles are in the 100-1000 nm range, with the contents of the vesicles being cytosolic components from the cell [17, 18].

Exosomes, also commonly referred to as small EVs (sEVs), are the smallest of the vesicle classifications and are the only subpopulation created through membrane invagination of the late endosomal membrane to form multivesicular bodies. These particles range from the lowest possible membrane structure size of around 30 nm to an upper size limit of 100 nm. Exosome cargoes are cell type dependent but are generally enriched in cargoes of both protein and nucleic acid origin, in addition to a diverse catalog of lipids spanning their membranes [17, 19, 20].

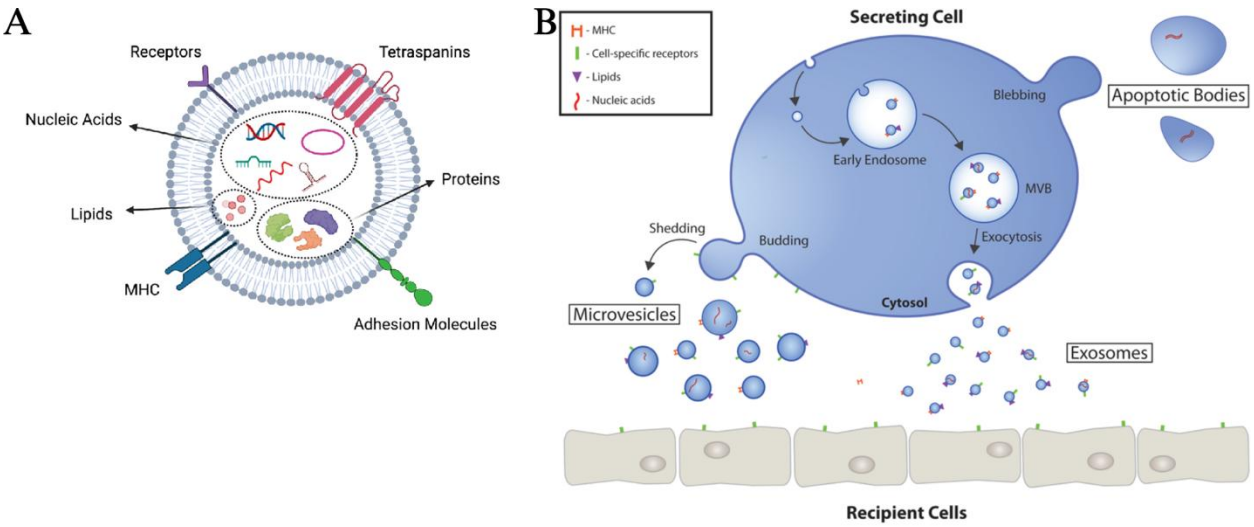

Figure 6 - Extracellular vesicle contents and classifications. (A) Representation of extracellular vesicle possible contents. EVs may contain in their lumen, membrane or surface any number of biologically active molecules. (B) The largest classifications of secreted vesicles are the apoptotic bodies, microvesicles and exosomes, which differ in size and method of secretion in eukaryotic cells [19, 20]. Created with BioRender.com.

1.6.2 PMSC EVs

Specific cell type confers cargoes and characteristics on their vesicles which can translate to specialized aptitudes for distinct therapeutic applications. In designing next generation therapeutics, the vesicle should be selected based on the translational capabilities of the native properties that the vesicle's cargo demonstrates. For applications in the CNS, vesicles from mesenchymal stem cells (MSCs) have been shown to have protective effects in murine models of CNS disorders, such as multiple sclerosis. The mesenchymal stem cell's secretome is enriched for bioactive molecules that can influence regeneration through paracrine signaling [21].

The extracellular vesicles derived from MSCs both retain many of the therapeutic benefits of their origin cell, as well as additional characteristics that make them the best choice for CNS disorder treatment. Growth factor cargoes of note that may be present within MSC EVs are brain-derived neurotrophic factor (BDNF), hepatocyte growth factor (HGF) and vascular endothelial growth factor (VEGF). Aside from BDNF's role in neuronal survival and proliferation, HGF is highly angiogenic with immunomodulatory effects by stimulating T-regulatory cells, which decrease chronic inflammation. VEGF is similar in its proangiogenic effects, but also has trophic effects on neurons and glia, inducing neurite outgrowth in the spinal cord [22]. Evaluating cell viability based on these growth factors, choice of cell is further narrowed to placental mesenchymal stem cells (PMSCs) due to higher secretion than bone marrow mesenchymal stem cells (BM-MSCs). In addition to their cargoes with regenerative properties, many EVs, including MSC EVs, can cross endothelial barriers. For disorders of the CNS, less invasive treatments that are not directly administered beyond these barriers, such as the Blood Brain Barrier (BBB), need to be able to cross biological barriers to deliver to their therapeutic target [21].

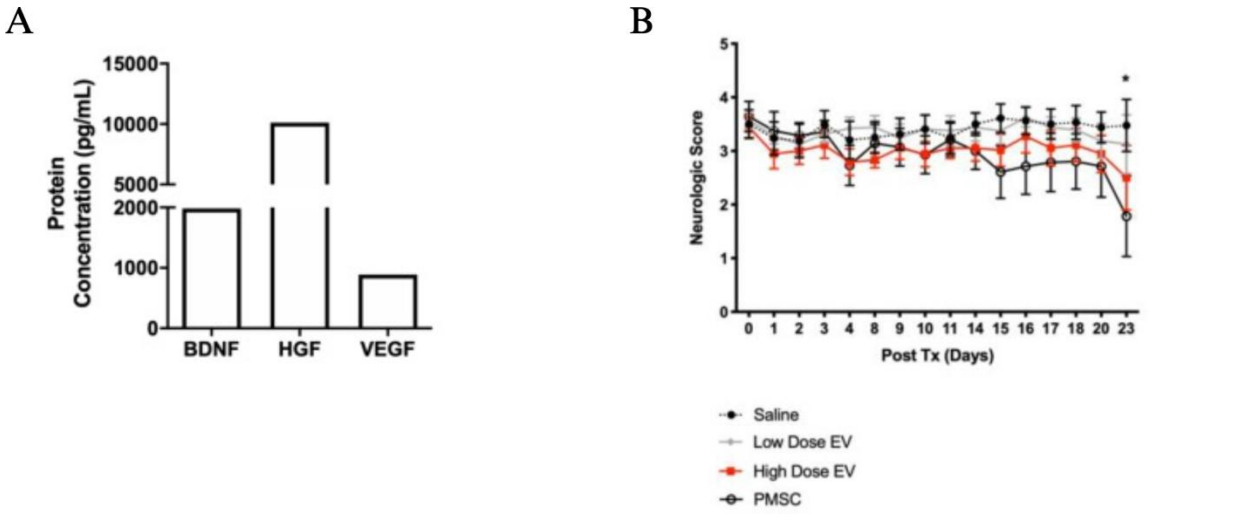

Figure 7 – MSC growth factors and MSC EV treatment profile. (A) Growth factors secreted in high concentrations in MSC cells that may be present in extracellular vesicles derived from them are BDNF, HGF, and VEGF. (B) In an induced autoimmune encephalomyelitis murine model of multiple sclerosis, mice were treated with saline, PMSCs and two treatment doses of PMSC derived EVs. High-dose and PMSC treatments both show an improved motor score in comparison to the saline treatment [21]. Created with BioRender.com.

Chapter 2: Materials and Methods

2.1 Thin Film Hydration and Extrusion

For experiments requiring thin film hydration and extrusion, processes were executed on two 1 mL Gastight Valco VISF-1 syringes (Hamilton Co, Cat: 81331) with 10 mm PE drain disc filter supports (Cytiva, Cat: 230300) and a 0.1 μm polycarbonate filter (Cytiva, Cat: 10419412) passed through the mechanism 11-21 times.

2.2 NanoAssemblr Ignite and Syringe Pumps

The organic phase was injected into the NanoAssemblr Ignite cartridge (Cytiva, Cat: NIN0061) with a BD 1 mL Luer-Lok Tip (Becton Dickinson and Co, Cat: 309628) syringe, while the aqueous phase was injected with a BD 3 mL Luer-Lok Tip (Becton Dickinson and Co, Cat: 309657) syringe. For the syringe pump system, an additional tubing was attached to the chip through a 1/16-inch LuerTight System (IDEX, Cat: P-837) and 1/16-inch PTFE laboratory tubing for microfluidics. The two syringe pumps used are a Genie Plus (Kent Scientific) and Series 100 pump (KD Scientific).

2.3 7,8-Dihydroxyflavone Preparation

The 7,8-DHF (Millipore Sigma, Cat: D5446-10MG) was suspended at 1 mg/mL in ethanol for reconstitution and further diluted to working concentration of 100 mg/mL for use in liposome formulations. Aliquots were stored at -20° Celsius between uses for a maximum of 3 months at a time.

2.4 Liposome Purification

Liposome purification was performed through both ultrafiltration and size exclusion chromatography. In experiments with purification through ultrafiltration, 0.5 mL Amicon Ultra Centrifugal Filter tubes with 100kDa molecular weight cutoff (Millipore Sigma, Cat: UFC5100) were used, spinning three times at 14,000 x g for 15 minutes with PBS washes in between. For SEC, 35 nm qEV original Columns (IZON, Cat: ICO-35) were utilized on a Version 1 Automatic Fraction Collector (IZON) run with PBS and one collection fraction of 0.8 mL with 0.87 buffer volume.

2.5 SY5Y Cell Culture

The human neuroblastoma cell line SH-SY5Y (ATCC HTB-11) was cultured in DMEM/F12 already supplemented with L-Glutamine and 2.438 g/L sodium bicarbonate (Gibco, Cat: 11320-033) with 10% fetal bovine serum (ATCC, Cat: 30-2020) and 1% penicillin-streptomycin (Gibco, Cat: 15140122). The cell culture was seeded, utilized and expanded from passage 8 to 12. Media was changed every 2-3 days until cells were at approximately 70-80% confluency and passaged.

2.6 EV Collection

HEK293 EVs were pelleted through ultracentrifugation through a standard protocol of two spins at 120,000 x g for 70 minutes on an Optima LE-80K Floor Ultracentrifuge (Beckman Coulter) occurring after the removal of whole cell, cell debris and aggregates by spins of 300 x g for 10 minutes, 2000 x g for 15 minutes, 10,000 x g for 30 minutes.

PMSC EVs were isolated through the Exodus H-600 (Exodus Bio) from PMSC UCD795 cell line in P5 and P6 with the large Exodus cartridge following spins of 500 x g for 10 mins, 2000 x g for 20 mins and vacuum filtering with 0.2 μm bottle top filter (Nalgene, Cat: 596-3320).

2.7 Neuroprotection Assay

During passage, cells were counted with a Countess Automated Cell Counter (Invitrogen) and SY5Y cells were plated on a 24-well plate (Cellvis, Cat: P24-0-N) at a density of approximately 100,000 cells per well in 500 µL of the DMEM/F12, 10% FBS, 1% penicillin-streptomycin media. After providing 24 hours to allow cells to adhere to the wells, staurosporine (Cell Signaling Technologies, Cat: 9953S) was added at .5 µL per mL of media per well. Following a 4-hour incubation period, the staurosporine containing media was removed, washed with warmed media, then media with treatment conditions were added. Following a 96-hour incubation, media was removed, and treated with Calcein AM (Invitrogen, Cat: C1430) and Hoechst 33342 (Invitrogen, Cat: H1399). Imaging was done using the Cytation C10 Confocal Imager (BioTek, USA) in the GFP, CY5, and DAPI channels at a magnification of 20x. 9 images were taken per well in a 3 by 3 grid and image analysis was done in program.

2.8 Nanoparticle Tracking Analysis

To determine concentration of liposomes, as well as corroborate DLS data of PDI and size, liposomes were diluted in 0.02 µm filtered (Whatman Anotop, Cat: 6809-1002) PBS (Corning, Cat: 21-040-CM) and analyzed through the NanoSight LM10 (Malvern Panalytical Ltd., UK) equipped with a 405 nm laser module, a sCMOS camera and an automated syringe pump (Harvard Bioscience, MA). The tubing was flushed with .02 µm filtered PBS prior to measurements. Liposomes are diluted 1000x before measurement of three, 90 second videos captured at camera level NanoSight NTA 3.1.4 and detection threshold of 5.

2.9 Dynamic Light Scattering (DLS)

Measurements were made on a Zetasizer Nano (Malvern Instruments) with samples diluted to 1 mL and measured in either disposable square polystyrene cuvettes (Sigma Aldrich, Cat: BR759030) or folded capillary cells (Malvern Panalytical, Cat: DTS1070).

2.10 Cryo-TEM

Carbon coated 300 mesh copper grids with 100 nm holes (Electron Microscopy Services, Cat: LC300-CU-100) were glow discharged for 25 seconds at 15 mA (PELCO easiGlow, Ted Pella). 4 µL of samples are loaded onto grids and then incubated for 2 minutes. Grids were then plunge frozen on the ThermoFisher Vitrobot IV, at 100% humidity and 22°C, blotted for 4 seconds at a force of +10. Grids were plunged into liquid ethane cooled by liquid nitrogen flash freezing them and then stored in liquid nitrogen. Samples were subsequently imaged on the ThermoFisher Glacios at 11,000× and 45,000× magnification. Images were analyzed through ImageJ by adjusting contrast and built-in measurement tools and against the machine's calibrated pixel size of 0.440 Å per pixel.

2.11 Statistical Analyses

Graphs, illustrations and statistical analyses were all completed in BioRender software. Bars represent the median of data points for graphs, and all data is analyzed with a $p < 0.05$ using either one way ANOVA or t-test where applicable unless indicated otherwise.

2.12 Neuron Quantification

In addition to the C10 image analysis, additional neuron quantification was completed by measuring projection lengths. This was accomplished through a Python script that isolated the green channel that stained for cell membrane and reduced the pixels to single pixel width

structures. These pixel structures were measured for their lengths and their values summed to assess an image's total neuron lengths.

Chapter 3: Results

To determine the effects of microfluidic loading the drug 7,8-DHF and formulation parameters on liposome and extracellular vesicles formulation, a number of characterization methods were conducted, including bulk and single particle analysis. Further neuroprotective assays were conducted to determine efficacy of the loaded 7,8-DHF in formulation.

3.1 Establishing and Optimizing Liposome Formulation

In evaluation of microfluidic formulated liposome characteristics for drug loading, the Ignite microfluidic platform (Figure 8A) was chosen for development based off the device's characteristics and manufacture scaling. Functionally, the Ignite is a highly controlled set of syringe pumps fed into a toroidal mixer microfluidic chip (Figure 8C). Due to the manufacturing scale intention of this device, cGMP standards were integrated into the design by making the chip single-use and disposable with chip tracking via RFID tags disabling use after a formulation in the machine. Since more investigation into formulation parameters were needed for this device, a reusable method was needed to increase the number of formulation cycles completed per chip. For this reason, a pump system was built outside the Ignite system (Figure 8B) and configured in a manner that mimics the native functionality (Figure 8D). When the same formulation was input into the Ignite and the syringe system, their respective resulting liposomes mean size was 84.61 nm in size with a PDI of 0.231 and 86.86 nm with a PDI of 0.238 (Figure 8E). Other parameters controlled by the Ignite, such as start/end waste and temperature were conserved outside of the machine with both having a start waste of .5 mL, no end waste and under ambient temperature.

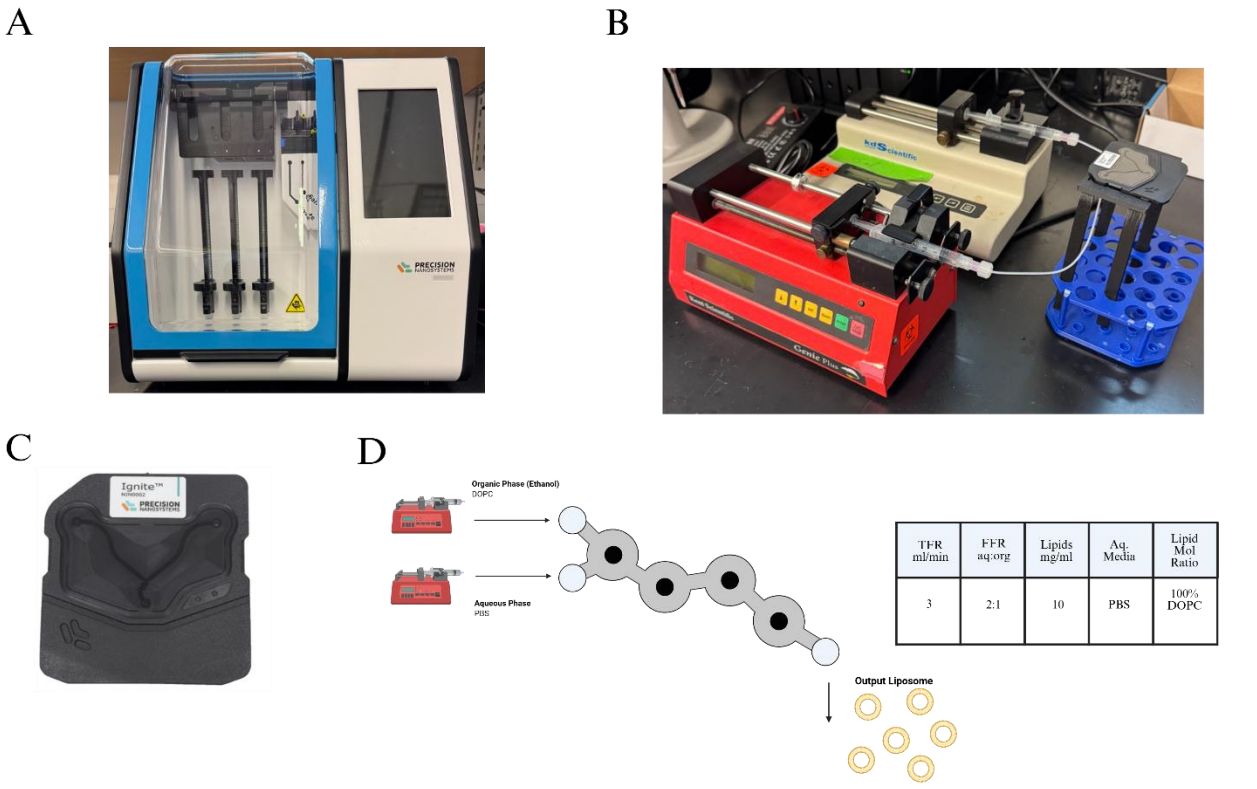

Figure 8 – NanoAssemblr Ignite and syringe pump system overview with associated liposome PDI and size profile measured through DLS. (A) NanoAssemblr Ignite nanoparticle formulation system from Cytiva and Precision Nanosystems. (B) Independent syringe pump setup that integrates two syringe pumps into the microfluidic chips for rapid and low-cost formulation prototyping. (C) NanoAssemblr Ignite formulation microfluidic chip. Two-inlet ports mixed through a toroidal pattern with one outlet. (D) Diagram of liposome formulation with DOPC and cholesterol inputs in the ethanol phase combined with the aqueous phase of PBS in both the NanoAssemblr Ignite and independent syringe pumps. (E) Comparison of PDIs of liposome populations for each system with the same formulation. (F) Comparison of the size of liposomes for each system. Created with BioRender.com.

3.2 Characterization of 7,8-DHF Liposome

Following assessment of the parameters input into the microfluidic mixer, the 7,8-DHF and the helper lipid cholesterol, was added into the organic phase with liposomes formulated according to the parameters laid out in Figure 9A and the resulting liposomes were characterized according to their downstream purification process (Figure 9B). Following mixing, a sample was taken for DLS to aid in the verification of liposome formation and measurement of diameter and PDI (Figure 10A and 10B). In the case of control liposomes with no added drug, the mean diameter was 103.1 nm with a PDI of 0.210. The 7,8-DHF added liposomes had a mean diameter of 81.09 nm with a PDI of 0.221 as measured on the DLS. Though the PDI did not show a statistically significant difference between the two conditions, the difference in diameter is significant with a $p < 0.01$.

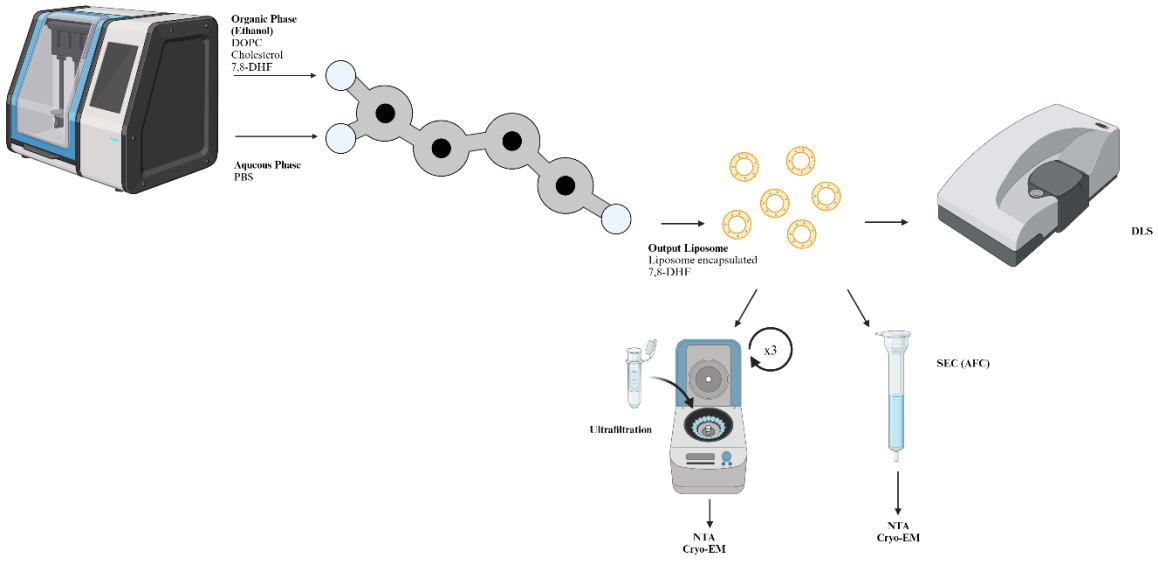

Figure 9 – 7,8-DHF loaded liposome formation and characterization overview. 7,8-DHF drug loaded liposomes are loaded via Ignite, evaluated on DLS then purified via ultrafiltration or size exclusion chromatography on an automated fraction collector. Purified samples are evaluated on NTA for concentration and bulk sizing and Cryo-EM for morphology and particle level characteristics. Created with BioRender.com.

After their purification methods of ultrafiltration and size exclusion chromatography, these nanoparticles were measured through NTA. The control liposomes purified through ultrafiltration

had a mean size of 114.0 nm with a standard deviation of 35.7 nm (Figure 10D). The 7,8-DHF loaded liposomes concurrently purified through ultrafiltration had a mean size of 120.3 nm with a standard deviation of 61.1 nm (Figure 10C). When control liposomes were purified through SEC, NTA results were a mean of 111.2 nm with a standard deviation of 30.8 nm (Figure 10F). The 7,8-DHF loaded counterparts were 107 nm with a standard deviation of 33.3 nm (Figure 10E). Between the two purification methods, SEC led to smaller resulting liposomes with decreased variance in sizing.

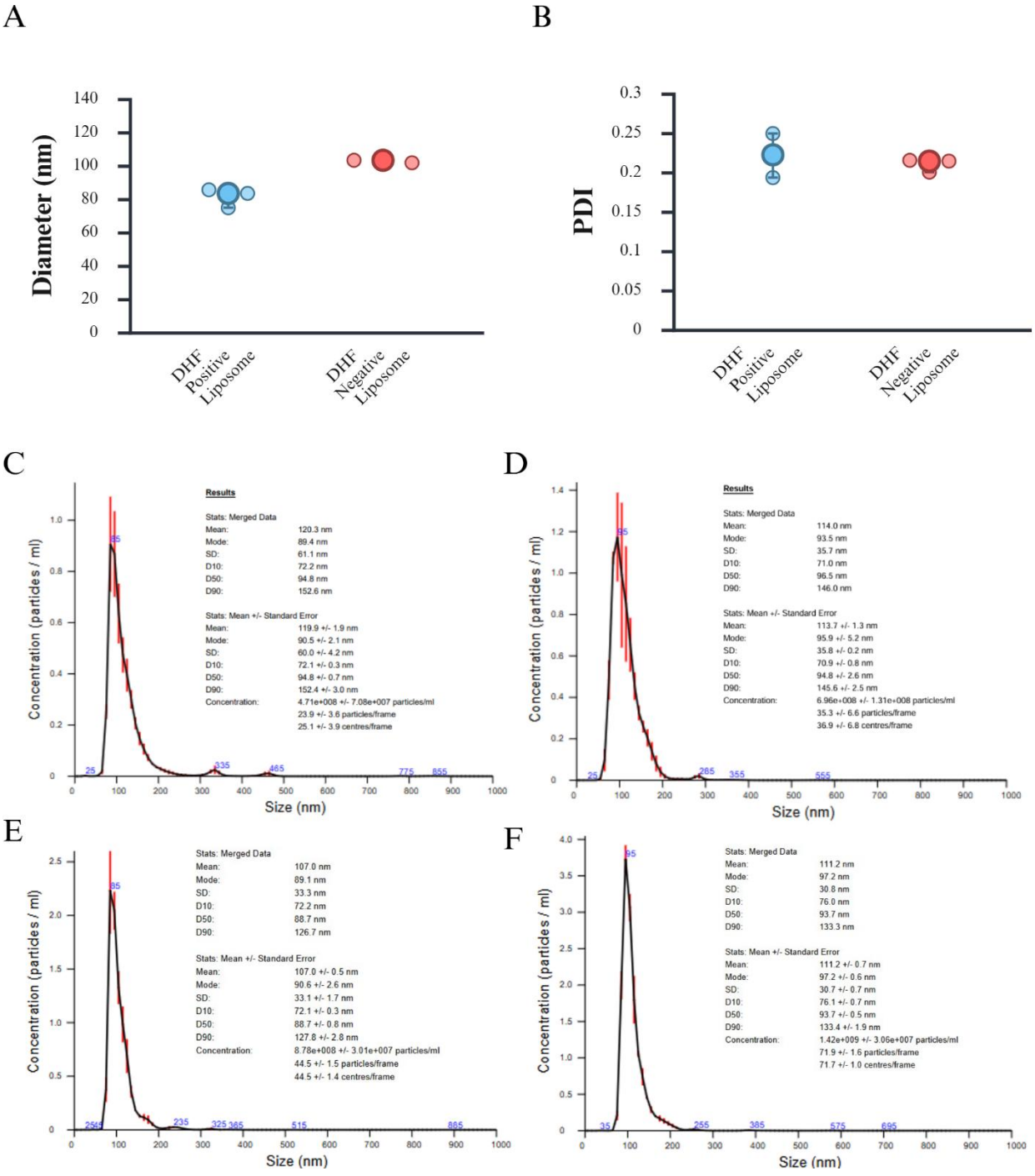

Figure 10 – Size and PDI profiles for liposomes. (A) Sizing of liposomes purified by ultrafiltration based on Dynamic Light Scattering. Statistically significant difference in sizing with $p < 0.05$. (B) Polydispersity Index (PDI) of drug loaded and not loaded liposomes purified by ultrafiltration based on Dynamic Light Scattering, but not statistically significant difference, $p > 0.05$. (C) NTA sizing of DHF drug loaded liposomes purified by ultrafiltration and associated statistical data acquired from the NanoSight. (D) NTA sizing of non-loaded liposomes purified by ultrafiltration and associated statistical data acquired from the NanoSight. (E) NTA sizing of DHF drug loaded liposomes purified by SEC and associated statistical data acquired from the NanoSight. (F) NTA sizing of not loaded liposomes purified by SEC and associated statistical data acquired from the NanoSight. Created with BioRender.com.

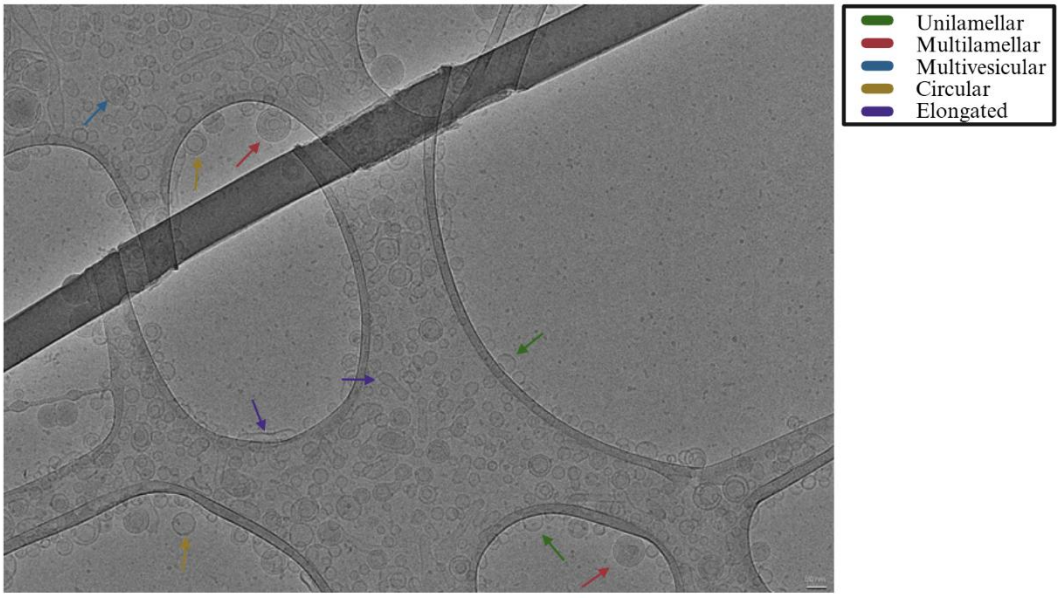

B

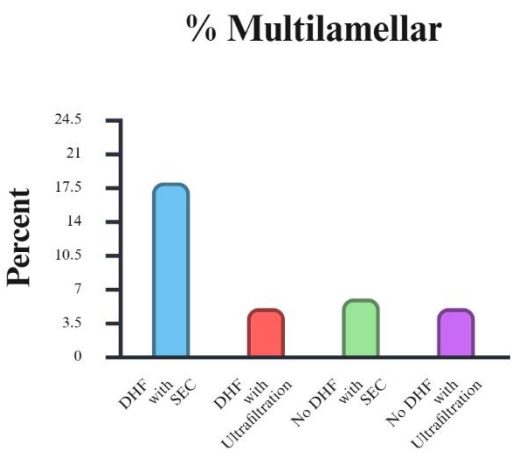

C

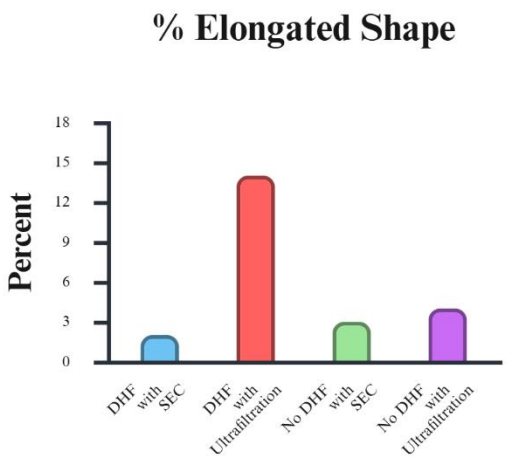

D

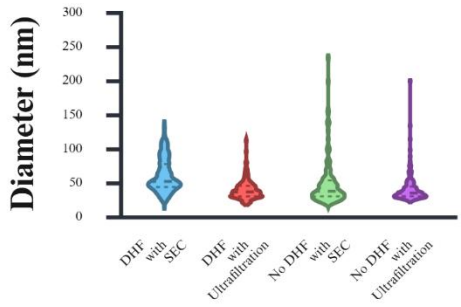

	DHF/SEC	DHF/Ultrafiltration	No DHF/SEC	No DHF/ Ultrafiltration
Average	60.52	48	39.1	40.8
Median	51.5	37.2	35.9	34.4
Standard Deviation	24.6	33.1	14.1	20.9

Figure 11 – Cryo-EM characterization of liposomes. (A) Cryo-EM image of non-DHF loaded liposomes purified via ultrafiltration imaged at 11,000x magnification. Arrows indicate examples of each classification for liposomes as unilamellar, multilamellar, multivesicular, circular or elongated by their respective colors of green, red, blue, yellow and purple. (B-C) Percent of liposomes matching designated morphological characteristic cataloged from one of each treatment condition (n > 180 for each condition). (D) Diameters of liposomes measured via ImageJ plotted and their averages, medians and standard deviations (n = 150 for each condition). Created with BioRender.com.

These four liposome populations were visualized through Cryo-EM to determine characteristics on a single particle level. The populations were evaluated based on diameter, lamellarity, presence of multivesicles and rough shape estimations with a binary between round or elongated. A representation of each of these descriptive categories can be seen in Figure 11A. For the descriptive characterizations such as vesicles, lamellarity and shape, all clearly distinguished liposomes in an image were categorized ($n > 180$) and their populations were evaluated regarding the total population of liposomes characterized normalizing for concentration differences.

The first of the characteristics, lamellarity, showed over 10% difference between the number of multilamellar particles in the liposomes loaded with 7,8-DHF and purified through size exclusion chromatography than the other liposome conditions. Secondly, shape also showed a near 10% increase in elongated liposomes in the group that has both 7,8-DHF and purification through ultrafiltration. Finally, size measured by diameter at the particles widest point, shows a larger range for liposome populations without 7,8-DHF, a higher portion of the liposomes having a diameter above 150 nm.

3.3 Neuroprotective Effects of 7,8-DHF Liposome

With physical characteristics of the liposomes determined, the neuroprotective function of the 7,8-DHF after encapsulation had to be measured. The ultrafiltration purified liposomes were utilized as shown in Figure 12A in comparison to no DHF added ultrafiltrate liposomes and free DHF (Figure 12B). Function was assessed through a staurosporine incubation of SY5Y cellular assay (Figure 12C-D).

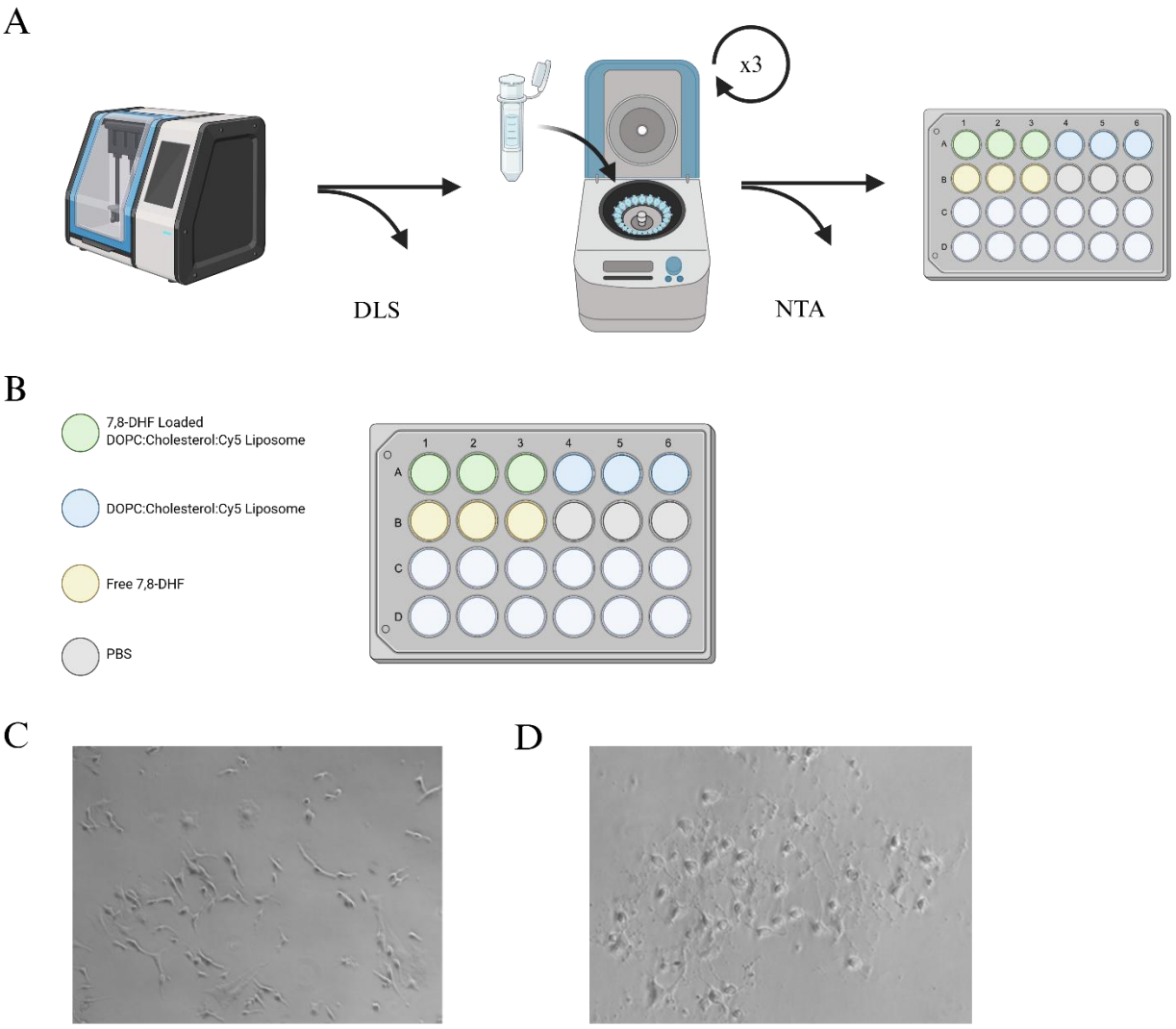

Figure 12 – Neuroprotection assay experiment overview. (A) Liposome formulation and processing workflow. Liposomes made in the Ignite, assessed via DLS, purified free frug and solvent through ultrafiltration, size and concentration assessed through NTA and then the appropriate concentration applied in the neuroprotection assay plate. (B) Neuroprotection assay plate for assessing loaded drug efficacy. (C) SY5Y cells in their healthy state before staurosporine introduction. (D) SY5Y 4 hours post-staurosporine introduction. Created with BioRender.com.

Following their 96-hour treatment incubation, the SY5Y cells were treated with Calcein AM, and Hoechst to image via confocal microscopy. Cells were then evaluated via three measurements: cell count, cell area and neuron projection lengths. For both cell count and cell area measurements, the confocal microscope's native analysis software was utilized with a primary and secondary mask implemented to decrease false positive measurements arising from dead cells and cellular debris abundant from staurosporine damage. Cell count was highest at an average of 131 cells observed over 9 images with the drug-loaded liposome treated cells,

seconded by the no drug liposome at an average of 59 cells observed per well. Both PBS and free 7,8-DHF had approximately 8-10 cells per image sample (Figure 13B). This cell count is significant between the drug and PBS conditions with a $p < 0.05$ and significant between the control liposome with a $p < 0.01$. The cellular area measurements showed similar increase in the drug liposome with an average of 2390 pixels per image in comparison to the no drug liposome treatment that measured at an average of 795 pixels per image (Figure 13C). These cell areas are significantly different with a $p < 0.01$ evaluated through the one-way ANOVA. Though the cell area measurement showed a less pronounced effect with no drug liposome in comparison to PBS and free drug with a nonsignificant difference between the groups. Free drug and PBS conditions measured an average of 440-566 pixels per image (Figure 13C). Like the cell count, the drug liposome and non-drug liposome differences were significant with a $p < 0.001$ and the difference between the drug liposome and the free 7,8-DHF and PBS was highly significant with $p < 0.001$. Like cell count, no effect could be seen by the free 7,8-DHF in comparison to the PBS treatment.

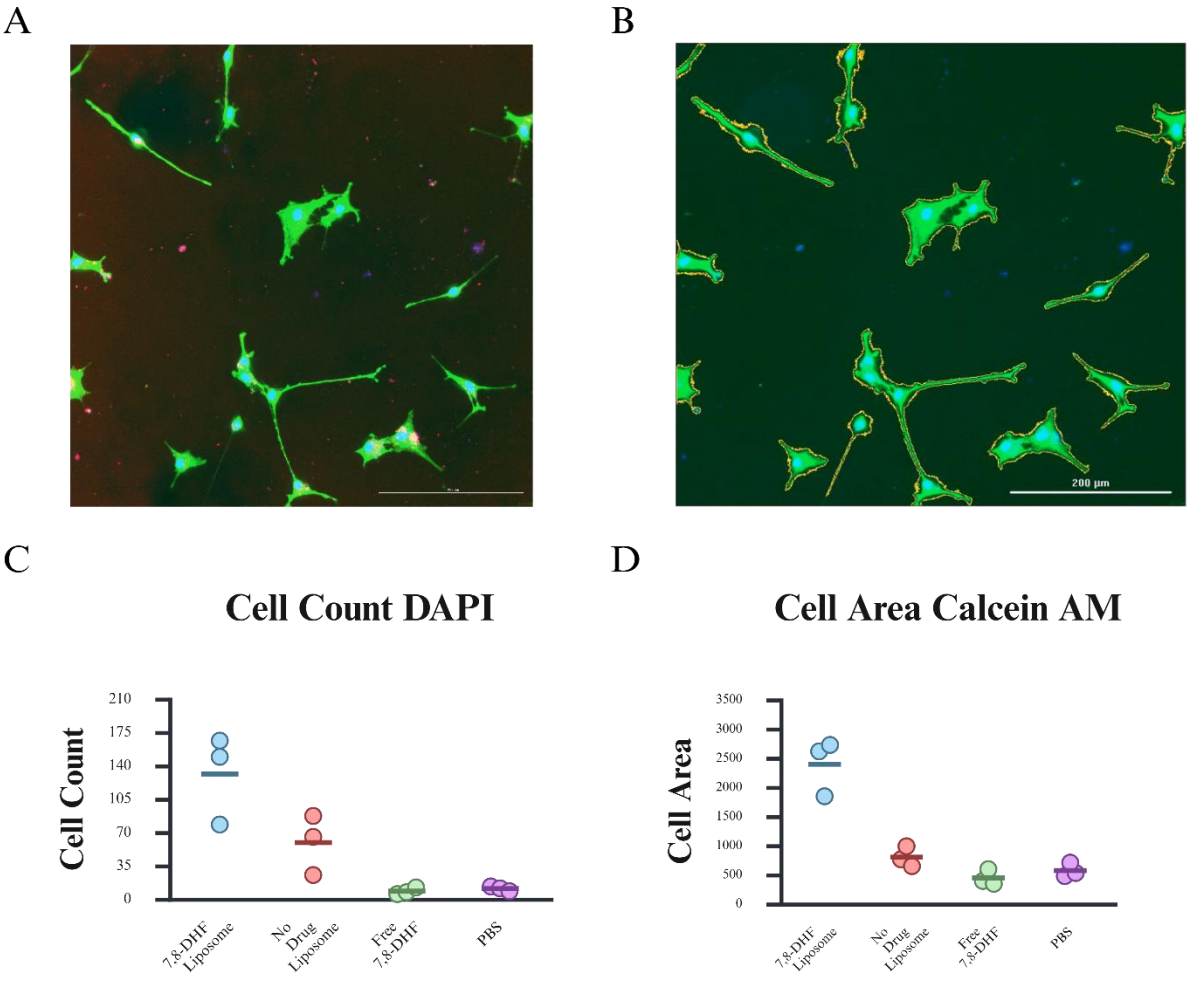

Figure 13 – Confocal images with cell count and cell area quantification. (A) Raw image captured on the C10 confocal microscope with the green channel being Calcein AM to stain cell membrane, the red channel is Cy5 which is incorporated into the liposomes to tag liposome localization, and the blue channel is Hoechst 33342 to stain nuclei through DNA binding. (B) C10 image processing primary mask of nucleus and secondary mask of Calcein AM which performs cell quantification that measures live cells by only measuring Calcein AM that is surrounding a Hoechst nuclear stained area and ignoring cell debris. (C) Cell count based on DAPI staining as the median of all 9 images taken per well (n = 3). (D) Calcein AM cell area calculated through the secondary mask and the median of the 9 images per well (n = 3). Created with BioRender.com.

The third metric, neuron length, was evaluated via a skeletonization method that measures specifically the Calcein AM channel for the cell membrane and generates a single pixel wide branching structure to measure neuron length with the ability to measure bends and multiple projections per neuron (Figure 14A-C). Neuron length followed cell count and area with the drug-loaded liposome treated images averaging about 3832 pixels while the no drug liposome images were the next highest at approximately 895 pixels per image. The free drug and PBS

treatments averaged roughly 170 pixels and 615 pixels per image respectively (Figure 14D). These differences between the drug loaded group and all the rest of the conditions were very significant with a $p < 0.0001$ measured by one-way ANOVA.

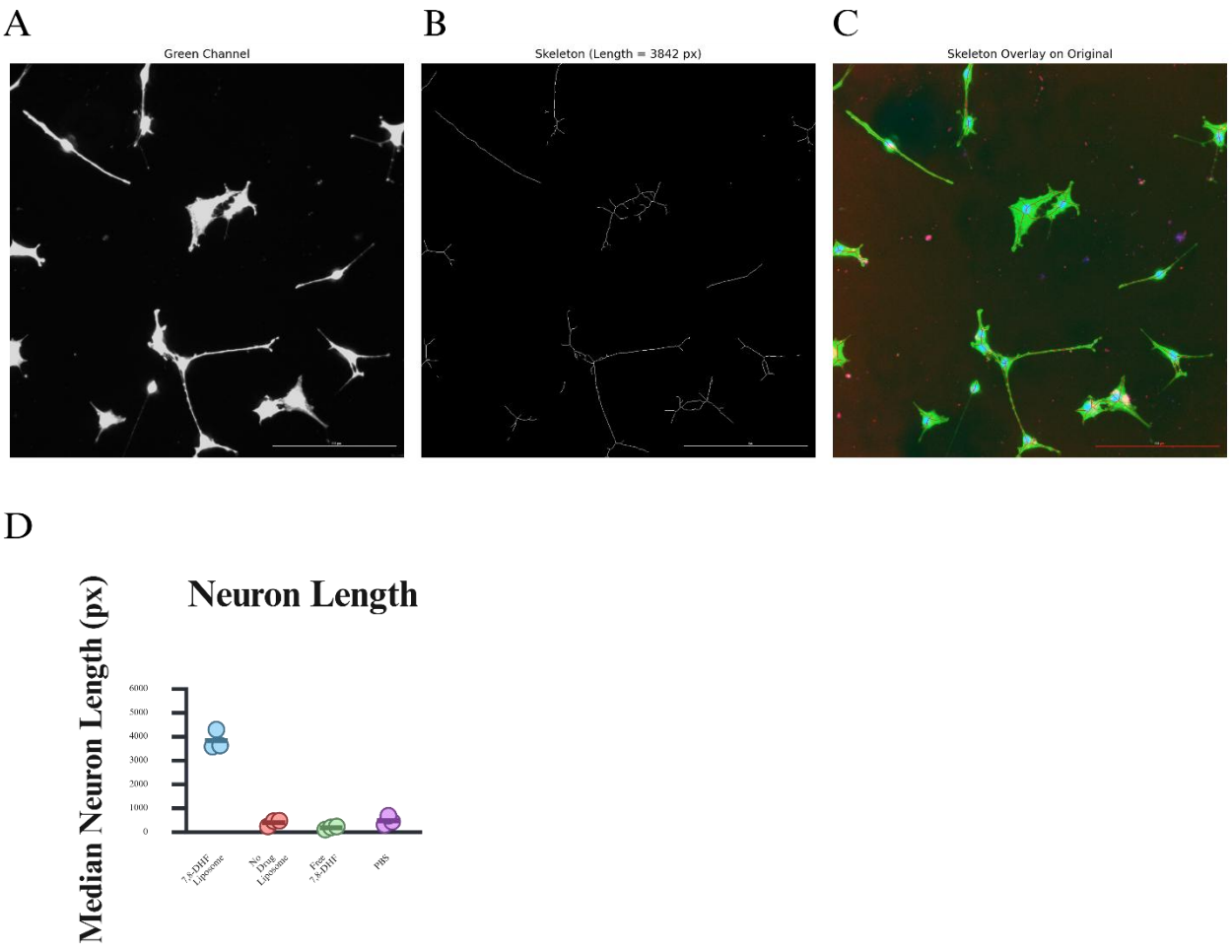

Figure 14 – Confocal images with neuron length quantification processing. (A) Green channel is isolated from the multichannel image to measure exclusively Calcein AM since it indicated cell membrane. (B) Skeletonization reduces objects to single pixel wide lines to reduce projections to their length and summed to calculate total neuron length per image. (C) Skeleton is overlaid original image in red to denote which cell bodies were measured. (D) Median neuron length in pixels is taken per well by taking medians of each of the 9 images taken per well (n = 3). Created with BioRender.com.

With preliminary evidence of drug-loaded liposome efficacy, further dose dependence evaluation was conducted to verify correlation between liposome concentration and neuroprotective efficacy. Repeating the previous methodologies, dose dependence was evaluated by cell count, cell area and neurite length (Figure 15A-C). With 10 times the initial treatment concentration, the

highest cell count was approximately 571 cells observed per well. However, cell area showed no positive trend with liposome concentration. Both cell count and cell area showed no significant differences betweeen treatments. The only measurment that showed differences between treatment conditions and even concentrations of treatment was the neuron length. There was a positive correlation between DHF concentration and median neuron length with the neuron length averaged between wells increasing with concentration to the peak of 10x with an average of 6218 pixels per well from the no 7,8-DHF added treatment condition average of 4367 pixels per well (Figure 15C).

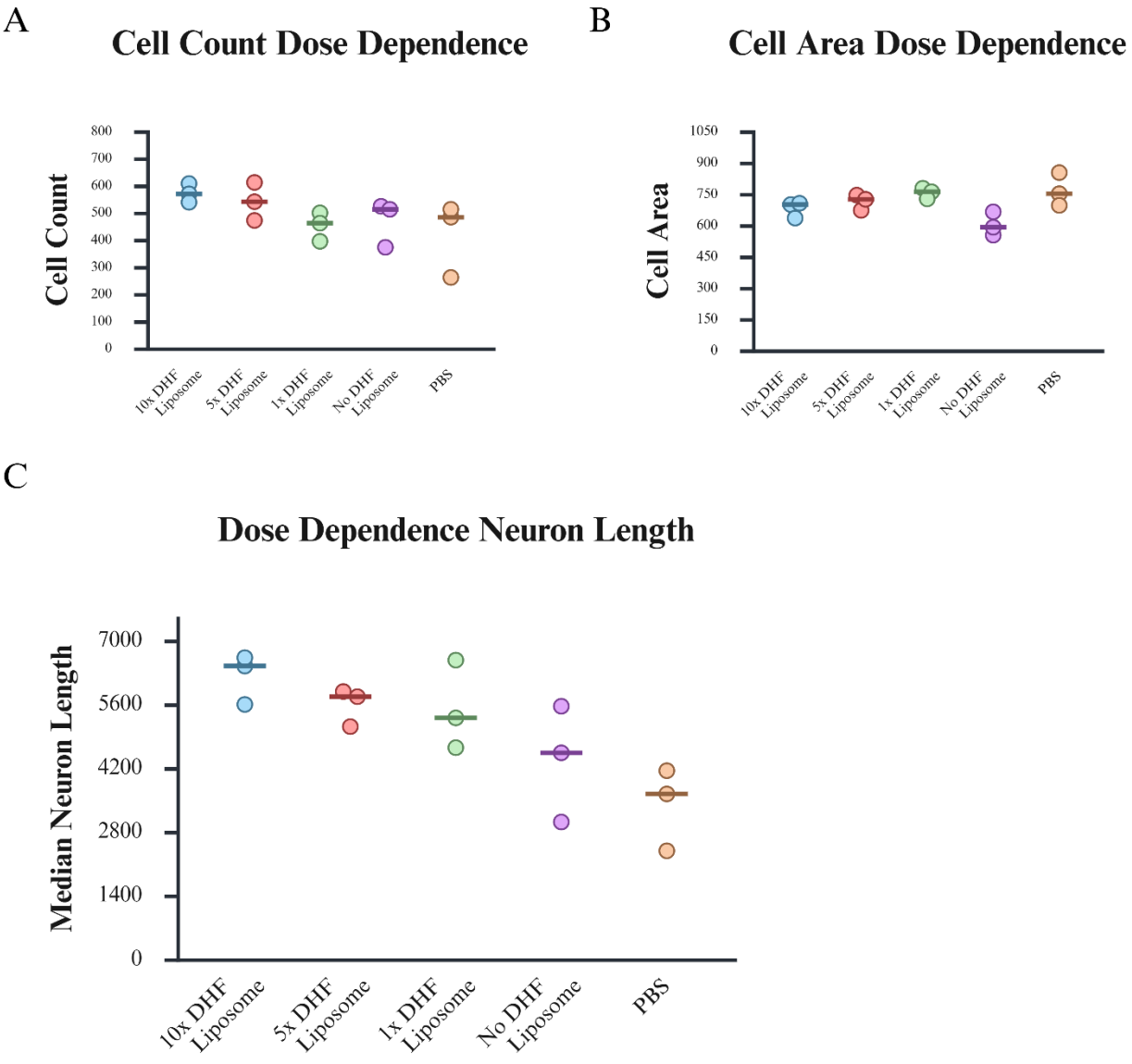

Figure 15 – Dose dependence quantification of cell count, area and neuron length. (A) Neuroprotection assay plate with labelled conditions for testing dose dependency. (B) Cell count as indicated by Hoechst 33342 quantified through the C10's image processing program and a median of 9 images taken per well in triplicate (n = 3). (C) Calcein AM cell area calculated through secondary mask under the same protocol with median of 9 images of each well in triplicate (n = 3). (D) Median neuron length measured through previously outlined skeletonization method in triplicate samples based on the 9 images taken per well (n = 3). Created with BioRender.com.

3.4 Neuroprotective Effects of PMSC EVs

The subsequent application for the Ignite platform following liposome formulations would be to apply microfluidic mixing to extracellular vesicles. The formulation and purification process was adapted and applied to PMSC EVs (Figure 16A). For sizing and concentration measurements to be used in the neuroprotection dosing, NTA was used to characterize the EV populations before

and after formulation. Following formulation and purification, the mean size dropped from 157.9 nm to 124.7 nm, as well as becoming less variant since the standard deviation went from 69.9 nm to 51.6 nm (Figure 16B-C).

A

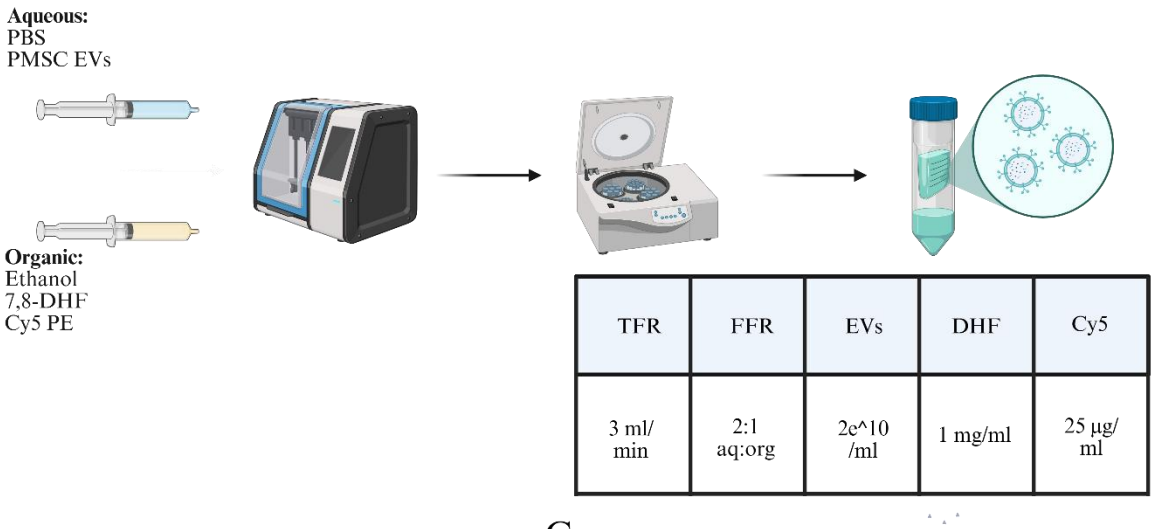

TFR	FFR	EVs	DHF	Cy5
3 ml/ min	2:1 aq:org	2e^10 /ml	1 mg/ml	25 µg/ ml

B

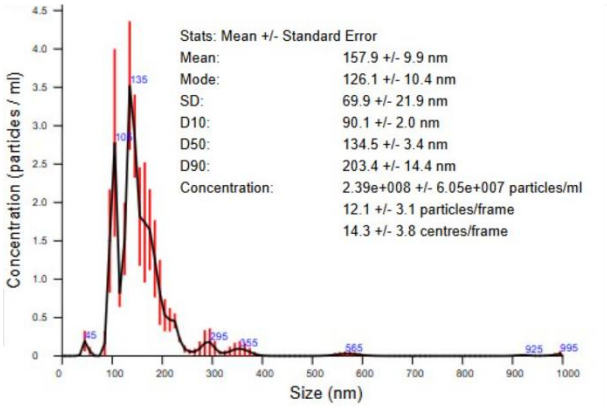

C

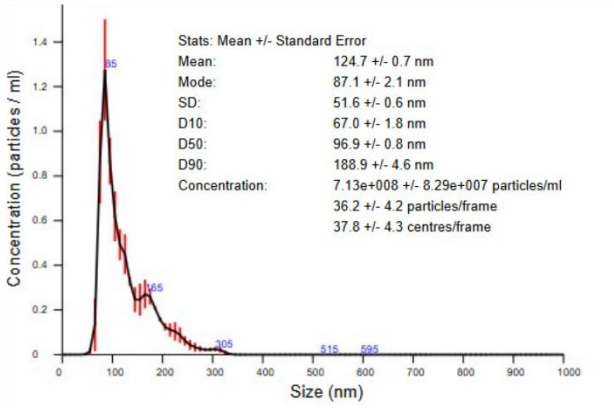

Figure 16 – EV loading process overview and NTA population profiles. (A) Formulation overview with key parameters such as fractional flow rate, EV and lipid fluorophore concentrations. (B) NTA size distribution preceding Ignite microfluidic injection. (C) NTA size distribution following Ignite mixing and ultrafiltration. Created with BioRender.com.

The neuroprotective assay conducted with these nanoparticles showed no improvement to cell count with either drug-loaded or control PMSC EVs. Though there is a slight improvement in PMSC neuron length conserved between both drug-loaded and non-drug-loaded extracellular vesicles, it is unfortunately a non-significant difference with a $p > 0.01$ (Figure 17C).

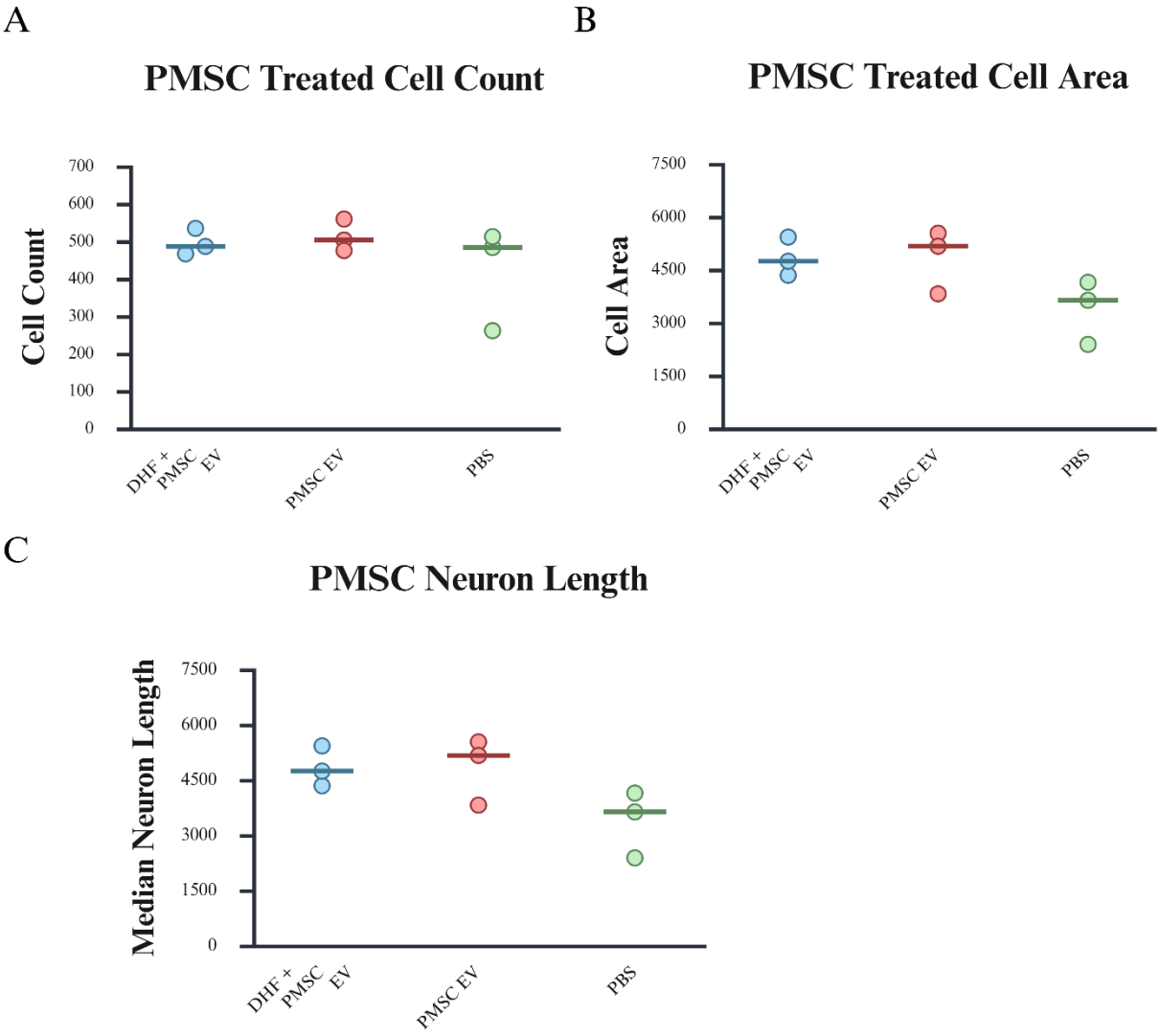

Figure 17 – PMSC EV quantification of cell count, cell area and neuron length. (A) Cell count as indicated by Hoechst 33342 quantified through the C10's image processing program and a median of 9 images taken per well in triplicate (n = 3). (B) Calcein AM cell area calculated through secondary mask under the same protocol with median of 9 images of each well in triplicate (n = 3). (C) Median neuron length measured through previously outlined skeletonization method in triplicate samples based on the 9 images taken per well (n = 3). Created with BioRender.com.

Chapter 4: Discussion

4.1 Syringe Pump System

Though the external syringe pump system was able to recreate the parameters used for subsequent formulations in the Ignite, the system's parameters functionality is significantly limited in comparison to the Ignite platform. The most significant difference in capabilities is the flow rates that can be achieved by the pumps on hand, and subsequently the volumes of materials the machine can handle. The device's flow rate limitations are correlated to the syringes utilized with larger syringes meaning a lower flow rate. Though the Ignite can use syringes up to 30 mL, the syringe pump system is restricted to 1 and 3 mL syringes to achieve the lower end of the flow rates achieved in the Ignite with a maximum total flow rate of 4 mL/min while the Ignite can reach a combined flow rate of 20 mL/min.

In addition to flow rate and material volume limitations, the type of lipids is also restricted based on phase transition temperature. In its current configuration, the syringe pump system is operating under ambient temperature, but some lipids, like sphingomyelin, require higher temperatures to remain in their liquid state in aqueous solvents. The Ignite system has integrated heating blocks to tune this parameter while the open-air nature of the syringe pump system means temperature controls would be needed for the entire environment.

The ability to tune these mixing parameters in liposome formulations may be extremely useful for medical applications as changes in total and fractional flow rates can contribute to smaller particle diameters [23]. A variety of lipid constituents could better mimic native vesicle populations or may endow the nanoparticles more beneficial functions in the body desired in

pharmaceuticals, such as higher efficiency in crossing endothelial barriers, specific tissue targeting, and avoiding immune and liver clearance.

4.2 Characterization of Liposomes and Neuroprotection

The necessity for single and bulk level characterization is apparent through the comparison between the single level characteristics evaluated through Cryo-EM and the population characteristics of DLS and NTA and corroborated through previous orthogonal analysis of EVs [24].

Unfortunately, there are major differences in data between the DLS, NTA, and Cryo-EM, especially when it comes to evaluating the sizing of the nanoparticles. This variance can be attributed to the limits of detection of the devices and the assumptions each machine makes about the measurements for each population. For the DLS and NTA, sizing for all populations were inflated in comparison to the Cryo-EM. Between all four conditions, even those with elongated liposomes, like those present in higher concentrations in the ultrafiltered 7,8-DHF loaded, showed a smaller average diameter measured when going from the NTA to the Cryo-EM. In NTA measurements, all four liposome bulk profiles indicated an average size in the realm of 107.0 – 119.9 nm, while the average sizes measured through Cryo-EM and ImageJ were 39.1 – 60.5 nm. These discrepancies may lead to differences in concentration from what was measured in the NTA, deviating from the treatment dose of 2000 particles per cell and increasing the dosage of liposomes per cell that was determined effective for EV dosing in previous neuroprotection studies.

In addition, there are differences in liposome morphology based on purification methods that are shown on the Cryo-EM images. The predominant differences between populations shown in this

medium is the number of elongated liposomes in the 7,8-DHF loaded ultra-filtered sample, the amount of multilamellar structures in the 7,8-DHF loaded SEC purified population, and the increase in range of diameters present in both the SEC and ultrafiltration populations without added 7,8-DHF. In both shape and lamellarity, only one population was significantly different from the rest while sizing differed between drug added and not added samples.

The elongated liposome shapes present in the 7,8-DHF loaded ultra-filtered purification population is a possible consequence of either centrifugation with the addition of the drug increasing membrane flexibility causing membrane fusions or increasing lipid and drug concentration during purification creating more sheet-like membrane structures when water concentration dropped significantly in the purified pellet. The centrifugation that comes from ultrafiltration adds an external mechanical stress to the liposome in the direction of centrifugal force towards the filtration tube walls, which could lead to liposomes shearing and combining in the direction of force. While the sheet-like structures is possible because ultrafiltration significantly drop the amount of water in the sample, leading to a loss of intraluminal water in circular structures and more liposomes breaking and reforming when diluted in later concentration preparations [25].

The multilamellar structures in 7,8-DHF loaded SEC purified are theorized to be a consequence of a combined effect of the drug and density gradient separation. The density gradient of SEC which may skew towards larger, denser multilamellar particles that are seen on the Cryo-EM images in the first fraction of the elution. In addition, smaller particles are more likely to be trapped in the SEC column that has 35 nm pores.

The consistently smaller diameters of liposomes with added 7,8-DHF are seen because the drug is incorporating into the liposome membrane area, as a nonpolar drug interacting with the

nonpolar tails of the lipid structures. Lipids like cholesterol function as helper lipids in liposome structures, decreasing the diameter that can be achieved, and 7,8-DHF may be reducing the strain of a small curvature and serving a similar function to cholesterol [26, 27].

The discrepancy in sizing in both average and range between these machines can be attributed to the limits of detection of these devices and how they process raw signal. For example, the limit of detection of the DLS used is lower than that of Cryo-EM at the magnification used but when processing data, the DLS assumes a homogenous sample with a normal distribution and can be skewed and obscured by larger particles. DLS is a bulk characterization method, so individual particles are not measured, rather the fluctuations in the scattering of light that correlates with a particle's Brownian motion and diameter. More rapid fluctuations in the intensity of light is indicative of smaller particles with a theoretical lower limit of measurement smaller than 1 nm when the sample is completely homogenous and uncontaminated [28]. The NTA sizing is similarly based off laser scattering and Brownian motion, however it's limit of detection is much higher and heavily dependent on the particle's refractive index. Smaller unlabeled biological particles, under approximately 70 nm, are difficult for the NTA to detect and measure, leading to a skew towards the larger particles [29].

The discrepancy in sizing that can be caused by these influences can be seen through the sizing results of liposomes both loaded and empty. Looking at just the 7,8-DHF loaded, and not yet purified samples measured by DLS, the sizing is given as a mean of 81.1 nm, while the 7,8-DHF loaded and ultrafiltered sample on NTA measured as a mean of 120.3 nm and a mean of 48 nm on Cryo-EM.

4.3 Neuroprotective Effects of 7,8-DHF Liposomes

The neuroprotective effect of 7,8-DHF loaded liposomes is investigated through measurements of cell count, cell area and projection length amongst several dosages and other treatment conditions with preliminary results based on the 2000 liposomes per cell baseline that showed improvement across all three performance metrics. Within these preliminary results, cell count, cell area and length all showed marked improvement indicating that 7,8-DHF was able to be loaded into the liposomes and the liposomes were interacting with cells in a manner that allowed for dispersal of its cargo. Progressing onto dose dependence, cell count and cell area no longer showed a significant improvement from the control groups but still maintained a dose dependence effect on neuron length. For more clarification on the dose dependence, another replicate of this experiment may need to be completed since the staurosporine may not have killed off enough of the cells to see a significant impact. This is a viable consideration for the lack of profound impact because all the performance metrics were significantly higher in the PBS control than seen in previous attempts at the assay.

4.4 Loading of PMSC EVs

As the final goal application for the Ignite system and 7,8-DHF would be to load the therapeutic into PMSC EVs with the expectation of a combined positive improvement from PMSC EVs and the drug, a preliminary loading was attempted with a subsequent neuroprotection assay. When attempting this, a similar workflow to the liposome formulation was implemented. Unfortunately, this workflow may not translate well to full formed and stable biological particles as the hydrophobic drug is incorporated in the hydrophobic tail region of the membrane of lipids during their self-assembly into liposomes. This may mean to fully encapsulate drugs in non-aqueous regions of the EV, a precursory detergent and solubilization step may be needed to

dissociate regions of the nanoparticle with a detergent like saponin or Triton X-100 [30]. As a result, this may be the reason why there was not an improvement in functionality between the loaded and unloaded PMSC EV in the neuroprotection assay.

In addition, the neuroprotection assay ran with these PMSC EVs may not show significant improvement since the PBS control being compared against shows limited deterioration. This assay was run in the same plate as the dose dependence liposomes (Figure 15) that showed improvement, but not as drastic as previous runs indicated. Along with this possible deficiency, the dosing between the liposomes and EVs concentrations may be different. Though they both were administered at 2000 nanoparticles per cell based on measurements made on the NTA, sizing and concentration measurements on the Cryo-EM were drastically different for liposomes and this may translate to inconsistent concentrations administered between EVs and liposome treatments. In this scenario, this could mean a higher concentration is needed for the PMSC EVs to reach a therapeutic dosage.

Conclusion

7,8-DHF may be a powerful therapeutic in the treatment of neuropsychiatric disorders, as well as spinal cord injuries, but that is dependent on the development of a next generation of therapeutic delivery agents capable of transporting hydrophobic substances with a higher tissue specificity and the ability to cross endothelial barriers while retaining therapeutic efficacy. For this purpose, liposomes and extracellular vesicles have been a prominent contender requiring more optimization and characterization of formulations and their mechanisms of action.

This research shows preliminary successes for loading the hydrophobic drug 7,8-DHF into liposomes, while maintaining the neuroprotective functionality with a mild dose dependence efficacy from 2000-10,000 liposomes per cell. Loading into PMSC EVs showed less success, with no significant improvement between loaded and unloaded EVs.

This research's significance lies in the ability to encapsulate hydrophobic drugs in liposomes, in a manner that is scalable for drug product manufacturing. Unfortunately, the main limitations thus far regarding this research has been the definitive correlation between dose dependence of liposomes and effective loading into extracellular vesicles in formulation of a higher throughput generation method, like the Ignite NP platform. In the future, following further optimization of extracellular loading through microfluidic platforms, the drug-loaded liposome should be applied to rodent models to prove the ability for the liposomes and extracellular vesicles to cross the blood-brain barrier and retain their pharmacological benefits.

References

[1] Y. Choi, “7,8-Dihydroxyflavone exhibits anti-inflammatory properties by downregulating the NF-κB and MAPK signaling pathways in lipopolysaccharide-treated RAW264.7 cells,” *Int. J. Mol. Med.*, Mar. 2012, doi: 10.3892/ijmm.2012.935.

[2] C. Liu, C. B. Chan, and K. Ye, “7,8-dihydroxyflavone, a small molecular TrkB agonist, is useful for treating various BDNF-implicated human disorders,” *Transl. Neurodegener.*, vol. 5, no. 1, p. 2, Dec. 2016, doi: 10.1186/s40035-015-0048-7.

[3] S. Yang and G. Zhu, “7,8-Dihydroxyflavone and Neuropsychiatric Disorders: A TranslationalPerspective from the Mechanism to Drug Development,” *Curr. Neuropharmacol.*, vol. 20, no. 8, pp. 1479–1497, Aug. 2022, doi: 10.2174/1570159X19666210915122820.

[4] E. Fliszár-Nyúl, V. Mohos, T. Bencsik, B. Lemli, S. Kunsági-Máté, and M. Poór, “Interactions of 7,8-Dihydroxyflavone with Serum Albumin as well as with CYP2C9, CYP2C19, CYP3A4, and Xanthine Oxidase Biotransformation Enzymes,” *Biomolecules*, vol. 9, no. 11, p. 655, Oct. 2019, doi: 10.3390/biom9110655.

[5] Z. Zhang *et al.*, “7,8-Dihydroxyflavone Prevents Synaptic Loss and Memory Deficits in a Mouse Model of Alzheimer’s Disease,” *Neuropsychopharmacology*, vol. 39, no. 3, pp. 638–650, Feb. 2014, doi: 10.1038/npp.2013.243.

[6] Y. Wang, J. Liang, B. Xu, J. Yang, Z. Wu, and L. Cheng, “TrkB/BDNF signaling pathway and its small molecular agonists in CNS injury,” *Life Sci.*, vol. 336, p. 122282, Jan. 2024, doi: 10.1016/j.lfs.2023.122282.

[7] S.-W. Jang *et al.*, “A selective TrkB agonist with potent neurotrophic activities by 7,8-dihydroxyflavone,” *Proc. Natl. Acad. Sci.*, vol. 107, no. 6, pp. 2687–2692, Feb. 2010, doi: 10.1073/pnas.0913572107.

[8] R. Raju, W. H. Abuwatfa, W. G. Pitt, and G. A. Husseini, “Liposomes for the Treatment of Brain Cancer—A Review,” *Pharmaceuticals*, vol. 16, no. 8, p. 1056, Jul. 2023, doi: 10.3390/ph16081056.

[9] P. Liu, G. Chen, and J. Zhang, “A Review of Liposomes as a Drug Delivery System: Current Status of Approved Products, Regulatory Environments, and Future Perspectives,” *Molecules*, vol. 27, no. 4, p. 1372, Feb. 2022, doi: 10.3390/molecules27041372.

[10] M. C. Smith, R. M. Crist, J. D. Clogston, and S. E. McNeil, “Zeta potential: a case study of cationic, anionic, and neutral liposomes,” *Anal. Bioanal. Chem.*, vol. 409, no. 24, pp. 5779–5787, Sep. 2017, doi: 10.1007/s00216-017-0527-z.

[11] A. Gabizon and D. Papahadjopoulos, “The role of surface charge and hydrophilic groups on liposome clearance in vivo,” *Biochim. Biophys. Acta BBA - Biomembr.*, vol. 1103, no. 1, pp. 94–100, Jan. 1992, doi: 10.1016/0005-2736(92)90061-P.

[12] A. Akbarzadeh *et al.*, “Liposome: classification, preparation, and applications,” *Nanoscale Res. Lett.*, vol. 8, no. 1, p. 102, Dec. 2013, doi: 10.1186/1556-276X-8-102.

[13] D. Lombardo and M. A. Kiselev, “Methods of Liposomes Preparation: Formation and Control Factors of Versatile Nanocarriers for Biomedical and Nanomedicine Application,” *Pharmaceutics*, vol. 14, no. 3, p. 543, Feb. 2022, doi: 10.3390/pharmaceutics14030543.

[14] A. Vogelaar, S. Marcotte, J. Cheng, B. Oluoch, and J. Zaro, “Use of Microfluidics to Prepare Lipid-Based Nanocarriers,” *Pharmaceutics*, vol. 15, no. 4, p. 1053, Mar. 2023, doi: 10.3390/pharmaceutics15041053.

[15] P. Ligrani, “A Study of Dean Vortex Development and Structure in a Curved Rectangular Channel With Aspect Ratio of 40 at Dean Numbers up to 430,” NASA, Contractor Report 19950005258, Jul. 1994. [Online]. Available: https://ntrs.nasa.gov/api/citations/19950005258/downloads/19950005258.pdf

[16] H. Bruus, “Governing Equations in Microfluidics,” in *Microscale Acoustofluidics*, T. Laurell and A. Lenshof, Eds., The Royal Society of Chemistry, 2014, pp. 1–28. doi: 10.1039/9781849737067-00001.

[17] M. A. Kumar *et al.*, “Extracellular vesicles as tools and targets in therapy for diseases,” *Signal Transduct. Target. Ther.*, vol. 9, no. 1, p. 27, Feb. 2024, doi: 10.1038/s41392-024-01735-1.

[18] H. Shao, H. Im, C. M. Castro, X. Breakefield, R. Weissleder, and H. Lee, “New Technologies for Analysis of Extracellular Vesicles,” *Chem. Rev.*, vol. 118, no. 4, pp. 1917–1950, Feb. 2018, doi: 10.1021/acs.chemrev.7b00534.

[19] D. Gustafson, S. Veitch, and J. E. Fish, “Extracellular Vesicles as Protagonists of Diabetic Cardiovascular Pathology,” *Front. Cardiovasc. Med.*, vol. 4, p. 71, Nov. 2017, doi: 10.3389/fcvm.2017.00071.

[20] A. R. Hart *et al.*, “The role of extracellular vesicles in endometrial receptivity and their potential in reproductive therapeutics and diagnosis,” *Reprod. Biol.*, vol. 22, no. 2, p. 100645, Jun. 2022, doi: 10.1016/j.repbio.2022.100645.

[21] K. Clark *et al.*, “Placental Mesenchymal Stem Cell-Derived Extracellular Vesicles Promote Myelin Regeneration in an Animal Model of Multiple Sclerosis,” *Cells*, vol. 8, no. 12, p. 1497, Nov. 2019, doi: 10.3390/cells8121497.

[22] Y. Han *et al.*, “The secretion profile of mesenchymal stem cells and potential applications in treating human diseases,” *Signal Transduct. Target. Ther.*, vol. 7, no. 1, p. 92, Mar. 2022, doi: 10.1038/s41392-022-00932-0.

[23] F. Yanar, A. Mosayyebi, C. Nastruzzi, D. Carugo, and X. Zhang, “Continuous-Flow Production of Liposomes with a Millireactor under Varying Fluidic Conditions,” *Pharmaceutics*, vol. 12, no. 11, p. 1001, Oct. 2020, doi: 10.3390/pharmaceutics12111001.

[24] N. M. Lowe *et al.*, “Orthogonal analysis reveals inconsistencies in cargo loading of extracellular vesicles,” *J. Extracell. Biol.*, vol. 3, no. 8, p. e70003, Aug. 2024, doi: 10.1002/jex2.70003.

[25] J. K. Koehler *et al.*, “Tailoring the Lamellarity of Liposomes Prepared by Dual Centrifugation,” *Pharmaceutics*, vol. 15, no. 2, p. 706, Feb. 2023, doi: 10.3390/pharmaceutics15020706.

[26] X. Cheng and R. J. Lee, “The role of helper lipids in lipid nanoparticles (LNPs) designed for oligonucleotide delivery,” *Adv. Drug Deliv. Rev.*, vol. 99, pp. 129–137, Apr. 2016, doi: 10.1016/j.addr.2016.01.022.

[27] M. Grit and D. J. A. Crommelin, “Chemical stability of liposomes: implications for their physical stability,” *Chem. Phys. Lipids*, vol. 64, no. 1–3, pp. 3–18, Sep. 1993, doi: 10.1016/0009-3084(93)90053-6.

[28] S. Falke and C. Betzel, “Dynamic Light Scattering (DLS): Principles, Perspectives, Applications to Biological Samples,” in *Radiation in Bioanalysis*, vol. 8, A. S. Pereira, P. Tavares, and P. Limão-Vieira, Eds., in Bioanalysis, vol. 8. , Cham: Springer International Publishing, 2019, pp. 173–193. doi: 10.1007/978-3-030-28247-9_6.

[29] V. Filipe, A. Hawe, and W. Jiskoot, “Critical Evaluation of Nanoparticle Tracking Analysis (NTA) by NanoSight for the Measurement of Nanoparticles and Protein Aggregates,” *Pharm. Res.*, vol. 27, no. 5, pp. 796–810, May 2010, doi: 10.1007/s11095-010-0073-2.

[30] S. Brezgin *et al.*, “Saponin is Essential for the Isolation of Proteins and RNA from Biological Nanoparticles,” *Anal. Chem.*, vol. 96, no. 43, pp. 17432–17443, Oct. 2024, doi: 10.1021/acs.analchem.4c04607.